POLITECNICO DI TORINO

Master's Degree in AEROSPACE ENGINEERING

Master's Degree Thesis

Conceptual design methodology and tools for the estimation of emissions from SABRE engine in rocket mode

Supervisors

Prof. Roberta FUSARO

Prof. Nicole VIOLA

Dr. Guido SACCONE

Ing. Valeria BORIO

Candidate

Alessio RICCA

JULY 2024

Summary

The increasing demand for access to space, driven by the steady growth of the space economy, shows the need to approach this sector with a different vision than that used to date. Historically, the space sector has always weighed in on technological solutions that maximize performance and minimize cost, but the growing demand for access to space and the goals of many current policies place a new focus on a new aspect, environmental impact. New solutions and strategies need to be developed to perform emission estimation early in the design phase so that the impact of technologies already in use and under development can be mitigated as much as possible. The present work operates in this direction: it is intended to develop an emission database of the Synergetic Air-Breathing Rocket Engine (SABRE), in its rocket mode, by applying NO_x emission estimation methods developed in civil aviation. The SABRE is the propulsion system and key component of the Single-Stage-To-Orbit (SSTO) Skylon aircraft that Reaction Engines Limited (REL) has been developing since 2009. It is an engine capable of operating in air-breathing mode up to an altitude of 25 km, at which altitude the transition to rocket mode takes place. It uses liquid hydrogen as fuel in both modes, while using air as an oxidizer in the air-breathing phase, so that it does not have to consume propellant stowed on board. When the air is too rarefied it proceeds to use the liquid oxygen contained in the tanks. The Skylon is a fully reusable horizontal takeoff and landing aircraft, and from this perspective it appears to be one of the most promising solutions for the future. Before it is possible to proceed with the emission analysis of this propulsion system, it is necessary to develop the thermodynamic model of the engine by which the propulsion database can be obtained. The results obtained will serve as input for the emission analysis from which the corresponding database will be obtained. Thermodynamic modeling of the SABRE needs to consider all the most important and characteristic aspects of this engine in order to make the propulsive database, and consequently the emission database, both reliable and consistent with reality. In particular, the helium regenerative cycle plays a major role. This is a solution that makes it possible to transfer, within the engine, large amounts of energy that are used to power the components therein or to regenerate other internal circuits, such as the hydrogen circuit. Accurate

modeling of the helium cycle is, therefore, of primary importance and is achieved by comparing different approaches and modeling of the noble gas. Emission analysis and database formation are obtained by considering the interaction of the wake, at high energy escaping from the engine, with the surrounding environment. In fact, the Skylon during the rocket mode emits only water vapor, hydrogen and oxygen, the latter in various forms, so in order to consider the impact of nitrogen oxides on the environment, it is necessary to analyze what happens during the interaction between the plume and the atmosphere. Cantera, a specific software capable of performing accurate analysis of both the mixing phase and combustion analysis in the main combustion chamber, is used within the model. In particular, the mixing phase is used both to analyze the interaction of the wake with the surrounding atmosphere and the mixing of the two propellants before Combustion Chamber (CC). In addition, this software allows the combustion to be modeled in chemical kinetics using 0D time-dependent simulations. An additional aspect that this work aims to investigate is the re-entry phase of Skylon, which is found to be highly relevant in the production of nitrogen oxides. The temperatures that develop during reentry are sufficiently high to occur the ionization of the air, therefore, during recombination, the presence of nitrogen atoms and ions, generate a production of nitrogen oxides that cannot be neglected.

Sommario

La richiesta sempre maggiore di accesso allo spazio, guidata dalla costante crescita dell'economia spaziale, mostra la necessità di approciarsi a questo settore con una visione differente da quella utilizzata finora. Storicamente il settore spaziale ha sempre peseguito soluzioni tecnologiche che massimizzassero le prestazioni e minimizzassero i costi ma la crescente domanda di accesso allo spazio e gli obiettivi di molte politiche attuali pongono in primo piano un nuovo aspetto, l'impatto ambientale. Nuove soluzioni e strategie devono essere sviluppate per effettuare una stima delle emissioni sin dalle prime fasi di progetto, in modo tale da poter mitigare al massimo l'impatto delle tecnologie già in uso e in fase di sviluppo. Il presente lavoro opera in questa direzione: si intende sviluppare un database emissivo del Synergetic Air-Breathing Rocket Engine (SABRE), nella sua modalità a endoreattore, applicando metodi di stima delle emissioni di NO_x sviluppati nell'ambito dell'aviazione civile. Il SABRE è il sistema propulsivo e componente chiave del velivolo Single-Stage-To-Orbit (SSTO) Skylon che la Reaction Engines Limited (REL) sta sviluppando dal 2009. Si tratta di un motore in grado di operare in modalità air-breathing fino ad una quota di 25 km, quota alla quale avviene la transizione alla modalità rocket. In entrambe le modalità utilizza l'idrogeno liquido come combustibile, mentre utilizza l'aria come ossidante nella fase air-breathing, in modo tale da non dover consumare propellente stivato a bordo. Quando l'aria è troppo rarefatta procede ad utilizzare l'ossigeno liquido contenuto nei serbatoi. Lo Skylon è un velivolo a decollo e atterraggio orizzontale completamente riutilizzabile e in quest'ottica risulta essere una delle soluzioni più promettenti per il futuro. Prima di poter procedere con l'analisi delle emissioni di questo sistema propulsivo è necessario sviluppare il modello termodinamico del motore mediante il quale ottenere il database propulsivo. I risultati ottenuti fungeranno da input per l'analisi emissiva dalla quale si otterrà il relativo database. La modellazione termodinamica del SABRE necessita di considerare tutti gli aspetti più importanti e caratteristici di questo motore in modo da rendere il database propulsivo, e di conseguerza quello emissivo, affidabili e attinenti alla realtà. In particolare, ricopre un ruolo di primaria importanza il ciclo rigenerativo dell'elio. Si tratta di una soluzione che permette di trasferire, all'interno del motore, ingenti quantità di energia che

vengono utilizzate per alimentare i componenti presenti o per rigenerare a sua volta altri circuiti interni, come quello dell'idrogeno. Una modellazione accurata del ciclo dell'elio è, quindi, di primaria importanza ed è ottenuta confrontando differenti approcci e modellazioni del gas nobile. L'analisi emissiva e la formazione del database sono ottenute considerando l'interazione della scia, ad alta energia che fuoriesce dal motore, con l'ambiente circostante. Infatti, lo Skylon durante la modalità a endoreattore emette solamente vapor acqueo, idrogeno e ossigeno, quest'ultimi in varie forme, perciò, per poter considerare l'impatto degli ossidi di azoto sull'ambiente è necessario analizzare cosa accede durante l'interazione tra i gas esausti e l'atmosfera. All'interno del modello è previsto l'uso di Cantera, un software specifico in grado di effettuare un'accurata analisi sia della fase di mixing che dell'analisi della combustione nella main combustion chamber. In particolare, la fase di mixing è utilizzata sia per analizzare l'interazione della scia con l'atmosfera circostante che per la miscelazione dei due propellenti prima della CC. Inoltre, questo software consente di modellare la combustione in cinetica chimica mediante simulazioni 0D dipendenti dal tempo. Un ulteriore aspetto che questo lavoro intende indagare è la fase di rientro dello Skylon che risulta essere altamente rilevante nella produzione di ossidi di azoto. Le temperature che si sviluppano durante il rientro sono sufficientemente elevate da verificare una ionizzazione dell'aria, perciò, durante la ricombinazione, la presenza di atomi e ioni di azoto, generano una produzione di ossidi di azoto che non può essere trascurata.

Table of Contents

List of Tables

List of Figures

Acronyms

AFT	Adiabatic Flame Temperature
AC	Air-Compressor
NH_4ClO_4	Ammonium Perchlorate
BC	Black Carbon
BFFM2	Boeing Fuel Flow Method 2
CO_2	Carbon dioxide
CO	Carbon monoxide
CC	Combustion Chamber
CEA	Chemical Equilibrium with Application
CFD	Computational Fluid Dynamics
C_D	Drag Coefficient
EI	Emission Index
FAR	Fuel-to-Air Ratio
GRAM	Global Reference Atmospheric Model
GWP	Global Warming Potentials
GHG	Greenhouse Gas
HX	Heat Exchanger
HRE	Hybrid Rocket Engines
N_2H_4	Hydrazine
HCl	Hydrochloric Acid
HTPB	Hydroxyl-Terminated PolyButadiene
HTOL	Horizontal Take-Off Landing
IATA	International Air Transport Association
IDT	Ignition Delay Time
ICAO	International Civil Aviation Organization
ISA	International Standard Atmosphere

RP1	Kerosene
LACE	Liquid Air Cycle Engine
LH2	Liquid Hydrogen
LOX	Liquid Oxygen
LRE	Liquid Rocket Engines
LEO	Low Earth Orbit
MR	Mixture Ratio
MMH	MonoMethyl Hydrazine
NASA	National Aeronautics and Space Administration
NIST	National Institute of Standards and Technology
NO_x	Nitric Oxides
N_2O_4	Nitrogen Tetroxide
PM	Particulate Matter
PBAN	PolyButadiene Acrynitrile
PB	Pre-Burner
PC	Pre-Cooler
RF	Radiative Forcing
REL	Reaction Engines Limited
SSTO	Single-Stage-To-Orbit
SOMA	Skylon Orbital Manoeuvring Assembly
SRM	Solid Rocket Motors
SSME	Space Shuttle Main Engine
Cp	Specific Heat at Constant Pressure
Cv	Specific Heat at Constant Volume
SABRE	Synergetic Air-Breathing Rocket Engine
UDMH	Unsymmetrical Dimethylhydrazine

Chapter 1

Introduction

In recent decades, access to space has become more and more frequent, with the number of annual launches growing exponentially, as shown in the figure 1.1, and will continue to grow in the near future due to the advent of the space economy [29].

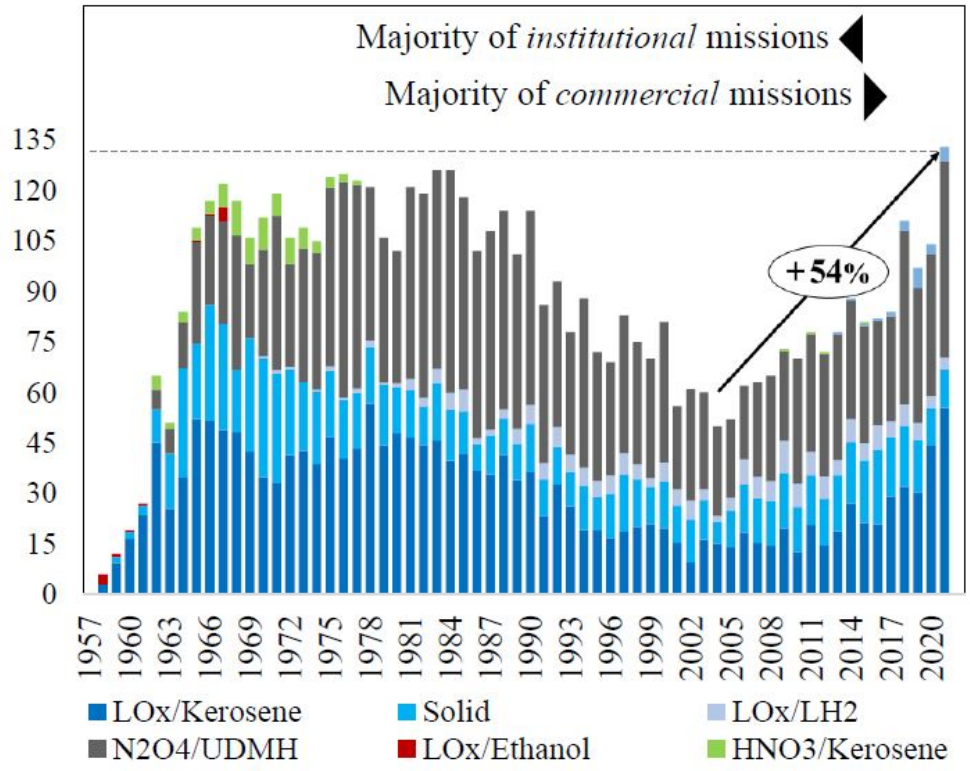

Figure 1.1: Trend of annual launches, [28]

Indeed, the development of new satellite constellations and space tourism will have a major impact on the number of launches per year. Currently, the aviation sector is responsible for 2.1% of carbon dioxide emissions generated by mankind in general, and 12% if only transport is considered [2]. Aviation emissions also include those emitted by launchers, but the latter are usually neglected due to their lower impact due to the volumes involved [25, 31]. However, considering the projected growth of the space economy [29] the environmental impact of launchers will no longer be negligible. Emissions generated by space access aircraft impact the environment in several ways: thinning of the ozone layer, changes in the energy balance of the atmosphere, or in the generation of mesospheric clouds [28]. Moreover, they are the only forms of man-made pollution in the upper layers of the atmosphere. Currently, there are no regulations or policies geared towards the control of launchers. However, two existing treaties can be applied to , the Montreal Protocol and the Paris Agreement. The former regulates the impact on the ozone layer while the latter is the international treaty on climate change. At the civil aviation level, the International Civil Aviation Organization (ICAO), International Air Transport Association (IATA) and other associations have created programmes that aim to minimise environmental impact, especially in terms of greenhouse gases [3, 4]. Therefore, in accordance with the above and with the aim of making aerospace transport more sustainable, it is essential to know and estimate the emissions for each type of aircraft in the atmosphere. In classical aviation, there are many methods of estimation, the most famous of which are the $P_3 - T_3$ and the Boeing Fuel Flow Method 2 (BFFM2) [5]. However, for the space access domain, the methods for estimating emissions generated by launchers or possible spaceplanes are very limited. In particular, the methods available for this type of analysis only allow for the calculation of primary emissions, i.e. those generated inside the combustion chamber, or secondary emissions, generated by the interaction between the wake and the surrounding atmosphere, but only thanks to semi-empirical relations, the reliability of which depends heavily on the data used to formulate them. Furthermore, this approach is only valid for technoloigical solutions similar to those used for data collection, which further limits applicability. Unfortunately, these are only useful in the last stages of the design process and not in the preliminary stages, where the study of emissions is essential in order to propose solutions that attempt to minimise them [14]. Therefore, the aim of this work is to develop a methodology for estimating Nitric Oxides (NO_x) emissions from space access launchers and, specifically, for the Skylon, a spaceplane Single-Stage-To-Orbit (SSTO) that will be able to land and take off horizontally. This aircraft is powered by two engines Synergetic Air-Breathing Rocket Engine (SABRE), positioned on the outside of the wings, which are able to operate in air-breathing mode up to a tangent altitude of 25km and then transition to a rocket mode. In particular, the model to be developed will refer to the latter flight mode of

the SABRE. The methodology that will be developed will try to be generalisable to any solution that can be adopted to access the Low Earth Orbit (LEO). The thesis will be divided into several macro-arguments organised by chapters: specifically, in the chapter 2, the state of the art of the current technologies available for accessing space and the emissions they generate will be presented. In addition, the few tools available for quantifying them will be presented and a comparison will be made with the estimation methods available for civil aviation. Chapter 3 will present in detail the SABRE, the case study adopted for this thesis work, and the reasons for this choice. Subsequently, in chapter 4, a brief overview of hydrogen will present the considerable benefits of this solution. However, there are also less positive aspects that need to be known and explored. In chapter 5, the propulsion model of the rocket-mode SABRE is realised, from which the propulsion database is derived. This will be useful both for the validation of the model, comparing the results with what is stated by the Reaction Engines Limited (REL), and for the realisation of the emission database, which will provide the emission indices of the products generated by the interaction between the engine's exhaust gases and the surrounding atmosphere, i.e., secondary emissions. Finally, in Chapter 6, the Skylon re-entry phase will be considered and the emissions generated during this phase will be estimated, particularly in terms of nitrogen oxides (NO_x). This will be done through both an analytical and numerical approach.

Chapter 2

State-of-Art in emission and propulsion modelling

The aim of this chapter is to examine the current state of available space access technologies and emission analysis methods. With this in view, it is intended to bring out the current limitations in technology and in analysing the environmental impact of launchers.

2.1 Current launcher technologies

Currently, the world landscape for access to space includes launchers and rockets with propulsion technologies that can be subdivided into four different categories according to the physical state of the propellants that power them: Liquid Rocket Engines (LRE), Solid Rocket Motors (SRM), Hybrid Rocket Engines (HRE) and, finally, solutions using hypergolic propellants. In all cases, chemical rocket propulsion is the only solution, of the available technologies, capable of generating sufficient thrust to reach orbit. Electric propulsion, although very efficient in terms of effective discharge velocity, generates thrusts in the order of a Newton which are not at all suitable for this purpose, while nuclear technology would theoretically be suitable, but the use of such technology would be risky for safety, as an accident would have very great repercussions. Despite the technology adopted, all launchers have one thing in common: a multi-stage configuration is always used. This is due to the fact that current technologies do not guarantee sufficient performance to reach orbital altitudes. Single-Stage-To-Orbit (SSTO) is currently being considered by designers but is not yet an adoptable solution due to the lack of technology that allows it to be realised. The following is a brief analysis of current technologies and their main characteristics [30, 6].

2.1.1 Liquid Rocket Engines

LRE use propellants, contained within pressurised tanks, to feed the Combustion Chamber (CC). Depending on the number of propellants used, they can be categorised as monopropellants or bipropellants. In the latter case, propellants consist of an oxidant, such as liquid oxygen, and a fuel, such as hydrogen or RP1. Monopropellants, on the other hand, are characterised by the fact that inside the tank they are in the form of a single molecule which, on reaching the combustion chamber and following a process of catalysis, decomposes and releases gases at high temperature: however, the performance of monopropellant solutions is particularly limited and in fact they are solutions usually adopted for attitude control. A classic schematic of an LRE can be seen in the figure 2.1.

It can be seen that there is a turbopump that compresses the propellants coming from the tank to inject them into the combustion chamber. This solution, which presents considerable benefits in terms of mass and performance, introduces an important issue that needs to be investigated in depth as it could lead to problems that could compromise the success of the mission: this is cavitation, a characteristic phenomenon of turbopumps, which consists of the formation of vapour bubbles inside the processed fluid that tend to collapse and generate strong stresses on the turbopump vanes. These stresses create problems in terms of both static strength and fatigue. What has aforementioned is not the only existing solution, but it is the one that is adopted in large propulsion systems that require continuous performance. Alternatively, there are *blowdown* or *repressurisation* systems that involve pressurising the tanks to values similar to those in the combustion chamber. In particular, the first is based on the emptying of the tank and the consequent decrease in pressurisation, while the second attempts to limit this loss in performance by using a second tank pressurised with inert gas which, once poured into the propellant tank, increases its pressure and consequently its performance. It is obvious how these technologies are limited for use in small propellers that do not have high performance or in the case of auxiliary thrusters. Therefore, in the following, reference will only be made to solutions that adopt an active thrust chamber supply system. In the thrust chamber, pressurised propellants are dosed, injected, atomised, mixed and burnt to form hot gases, which in turn are accelerated and ejected at high speed through a supersonic nozzle, thus imparting thrust to the vehicle. In fact, a rocket engine thrust chamber can be divided into three main parts: injectors, a combustion chamber and a nozzle. One of the main benefits of this solution is the possibility of thrust adjustment, shutdown and subsequent re-ignition of the engine. If these engines are to be used for a very long time, cooling solutions must be considered for both the combustion chamber and the nozzle. Indeed, the gases generated as a result of combustion reach very high temperatures that would affect the structural integrity of the engine and its components. The most widely

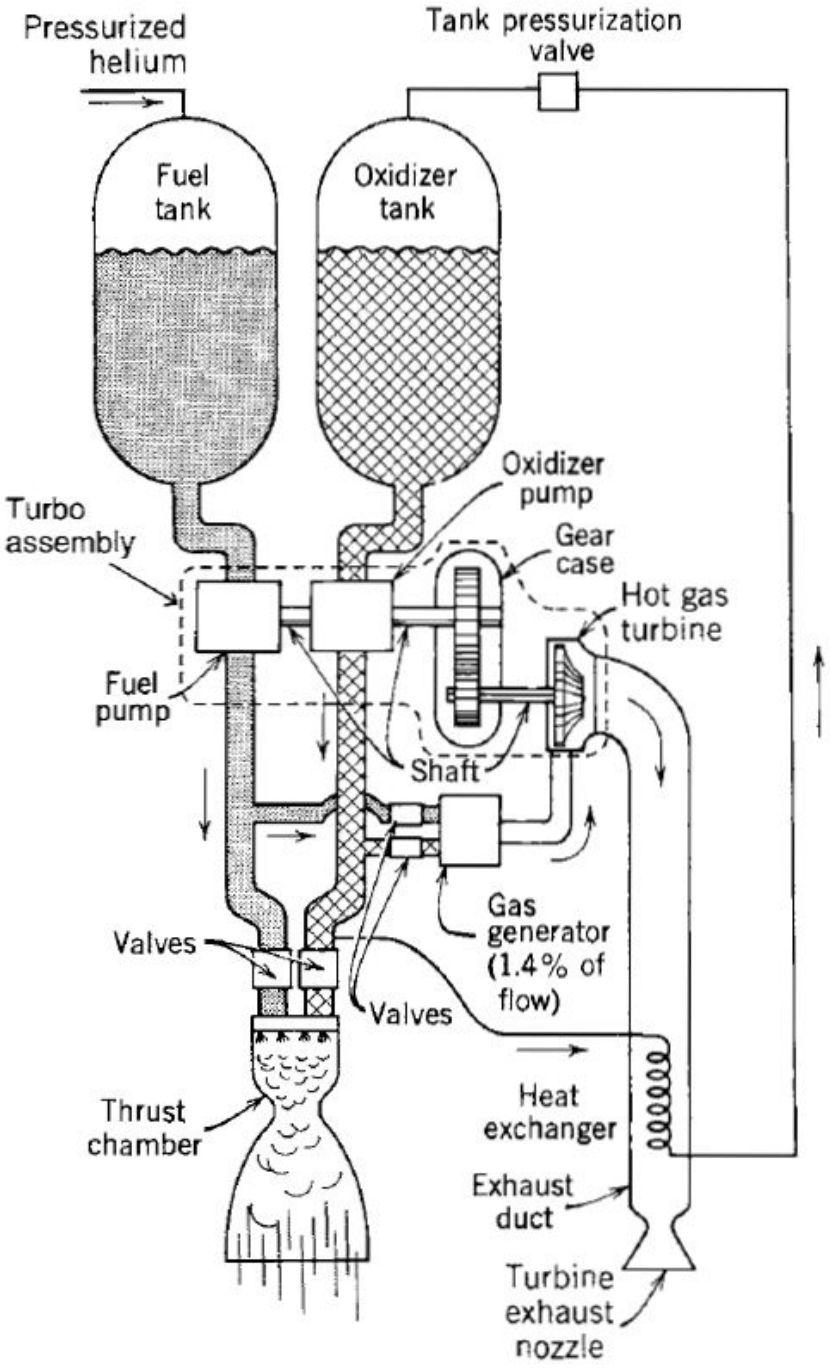

Figure 2.1: Classic scheme of a LRE, [30]

adopted solution for cooling the combustion chamber involves using the fuel itself as a coolant, which, by receiving regeneration, will ensure higher performance. For the nozzle, on the other hand, there are different solutions depending on the use and stage of the nozzle in question. Active cooling is typical in the case of the first stage of a launcher, while the use of high-emissivity materials to exploit radiation is typical in the case of nozzles used in the upper stages. For the most developed thrusters, it is possible to integrate other systems to manage thrust orientation and to handle residual propellants in the case of re-ignition: in addition to the main thruster, there are several smaller thrusters whose task is to manage and stabilise the propellant in special devices, such as traps, 'vanes' or sponges. These devices are capable of retaining a minimum amount of propellant necessary to perform a re-ignition and allow the remaining propellant to be arranged in such a way as to ensure a continuity of supply. The performance of this type of solution varies considerably depending on the combination of propellants used and the size of the launcher. In fact, it is a very scalable technology capable of generating thrust over a very wide range, from small fractions of a newton to tonnes of thrust required to reach orbit. In terms of specific impulse, chemical propulsion, and in particular liquid propulsion, is inferior to many other technologies, as can be seen in the figure 2.2, but because of its high thrust-to-weight ratio, it is the only useful solution for escaping the Earth's atmosphere.

2.1.2 Solid Rocket Motors

SRM are the other main solution currently in use. These engines consist of a single body, the *case*, which contains the combustion chamber and nozzle within it. The propellant, termed *grain* for this type of thruster, is contained directly in the combustion chamber, as can be seen in the figure 2.3. The operation of SRM is quite simple: the igniter, electrically activated, supplies sufficient energy to the engine to start combustion on the exposed surface of the grain. This begins to burn exposing new layers to combustion, until the propellant is completely consumed. During combustion, high-energy gases are developed and directed towards the supersonic nozzle, which, by expanding them, generates thrust. This technology is usually used in parallel with liquid propellant-fuelled launchers as boosters.

In order to present this technology in the best possible way, we proceed by making a direct comparison with the characteristics of LREs. This will make it simpler to understand the advantages and disadvantages of this solution. In particular, the advantages are:

- Ability to be stored for long periods without compromising their performance and safety in use. LREs, on the other hand, especially in the case of cryogenic propellants, present considerable problems in this aspect. The transition from

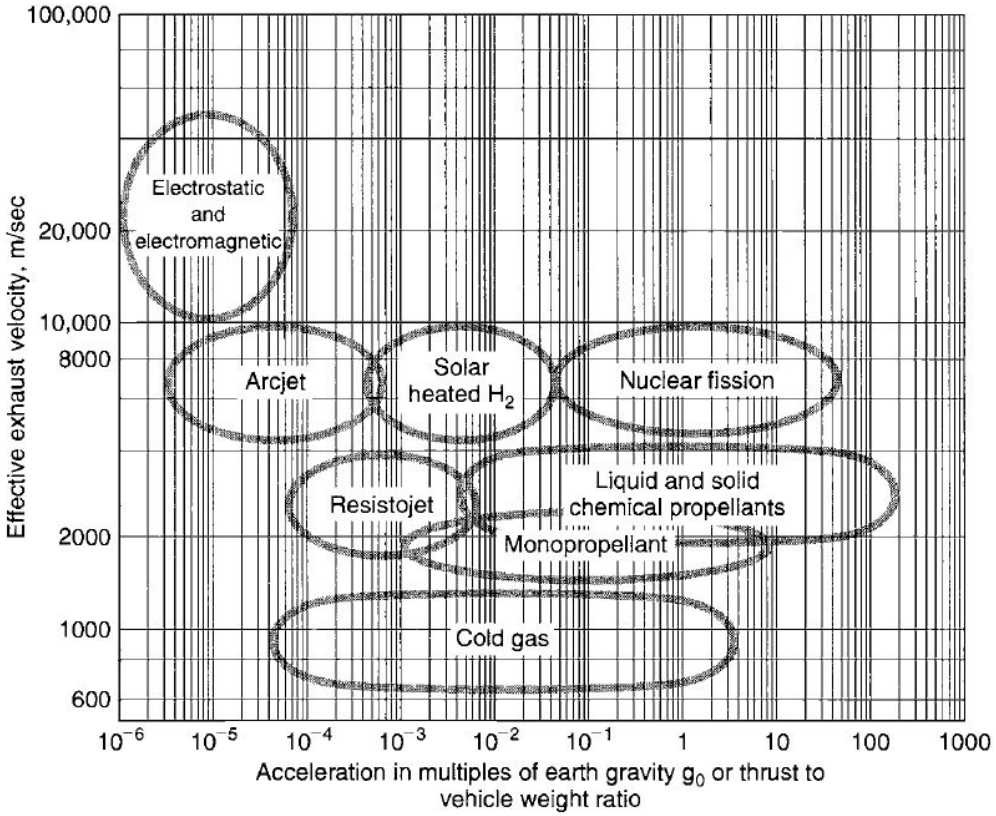

Figure 2.2: Diagram of launchers as a function of thrust-to-weight ratio and specific impulse, [30]

a liquid to a gaseous state is a non-negligible aspect, and in order to avoid excessively high pressure rises, part of the propellant is emptied by means of safety valves, resulting in a loss of performance;

- The propellants used, as long as they are in a solid state, are harmless to humans and are therefore safer during manufacture and transport, unlike many liquid propellants used in the technology described above;
- The absence of many components found in LREs, such as the fuel system, turbopumps, and active cooling systems: they are therefore simpler and cheaper solutions;
- Lastly, they are particularly reliable and, above all, ready for immediate use: in fact, they do not require any special take-off preparation procedures.

However, these solutions also have many limitations, such as:

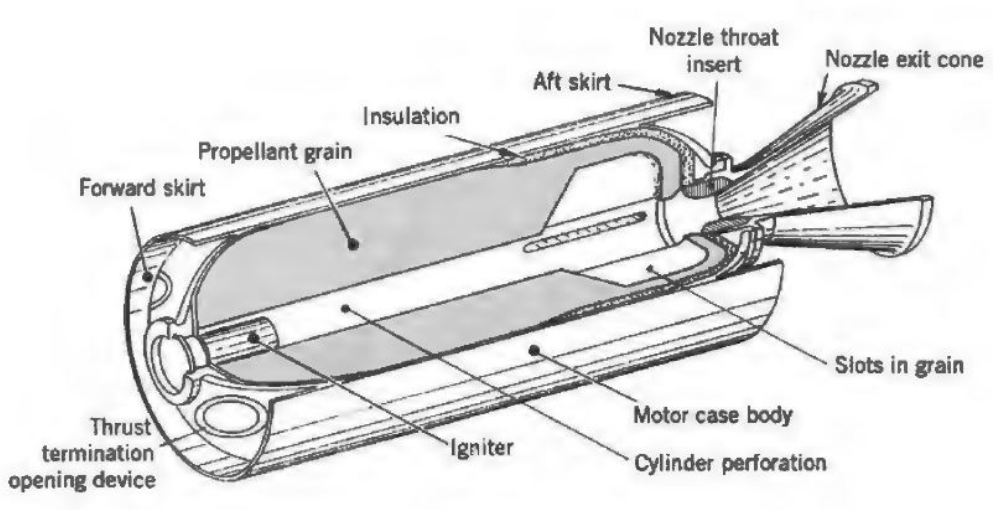

Figure 2.3: Classic scheme of a SRM, [30]

- Relatively low specific impulse values, although partly compensated by the high impulse-density ratio;
- Under certain temperature and pressure conditions, the grain used could become brittle and capable of cracking. These cracks created could generate pressure increases capable of destroying the launcher itself;
- Thrust regulation and its orientation are solutions that are difficult to implement in this technology;
- Turning this type of engine off and on is difficult if not impractical;
- Thermal management of the nozzle is a particularly delicate aspect. The absence of active cooling systems, due to the absence of a liquid propellant capable of acting as a heat sink, makes it one of the most critical elements within the engine;
- Combustion instability. This aspect is one of the most problematic and depends mainly on the combustion rate and in particular its exponent. To achieve stable combustion, it is necessary for this exponent to be less than unity. In fact, in this case it would be observed that, for small variations in pressure in the combustion chamber, there would be a balancing due to the difference in the flow rate coming out of the nozzle compared to that generated in the combustion chamber which tends to bring the pressure back to the designated operating point. Conversely, if the exponent were greater than unity, the operating point would be an unstable equilibrium point and, consequently, for small disturbances, unstable combustion would result.

Some of the flaws just presented can be managed by various solutions that can be adopted in these engines. For example, the management of the thrust profile can be performed through the design of the *grain*. Looking at the figure 2.4, it can be seen that, depending on the shape assumed by the *grain*, different thrust profiles occur that can be functional for different missions. This is due to the fact that the area of burning surface varies, which is in turn dependent on the *grain*'s rate of regression and, indeed, on the initial geometry: in fact, the pressure that develops in the chamber, and therefore the resulting thrust, is a direct function of the burning surface. However, it is not possible to actively and instantaneously adjust the thrust, as the thrust profiles are defined at the moment the *grain* is built and introduced into the *case*. Moreover, the thrust profiles that can be obtained by manipulating the *grain* geometry are limited because, going back to the issue of the fragility of propellants, it is not possible to consider excessively articulated shapes as this would risk damaging the *grain* itself.

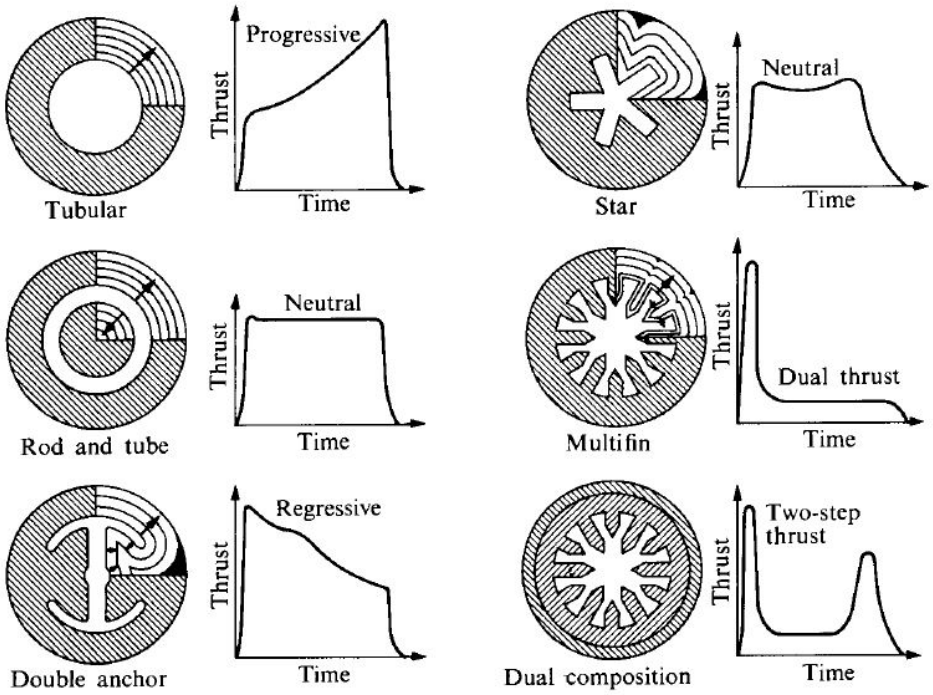

Figure 2.4: Typical *grain* geometries for different thrust profiles, [11]

The design of the nozzle must take different aspects into account. In particular, the use of materials that are resistant to the very high temperatures that are reached due to the lack of active refrigeration methods must be provided for. In addition, since there are solid elements in the grain that are released into the combustion gases as particles during combustion, erosion of the nozzle and in

particular of its throat section must be foreseen. The eroded materials and these high-temperature solid particles can also settle on the walls of the nozzle and generate asymmetry in the flow. The propellants used can be categorised into two main types: homogeneous and composite propellants. An intermediate form are those solutions involving the use of homogeneous as bases for propellants of the second type. The best known and most widely used homogeneous propellant is the combination of *nitrocellulose* (NC) and *nitroglycerine* (NG). Composite propellants, on the other hand, consist of inorganic salts, used as oxidisers, and fuels or binders such as plastics or rubbers. Usually, metal powders, such as aluminium, are added to the binder, which improve performance but generate residues that are very harmful in terms of environmental impact. The last aspect to consider is that these carriers are usually considered expendable and consequently their polluting impact increases considerably.

2.1.3 Hybrid Rocket Engines

An intermediate solution that attempts to combine the advantages of the two previously proposed technologies involves the use of a solid propellant, usually the fuel, and a liquid propellant, usually the oxidant. This solution is rather old, but has recently come back in vogue as the technologies now available enable fairly high performance to be achieved, but still lower than that obtained by LREs alone. In the figure 2.5 it can be seen the classic design of these engines.

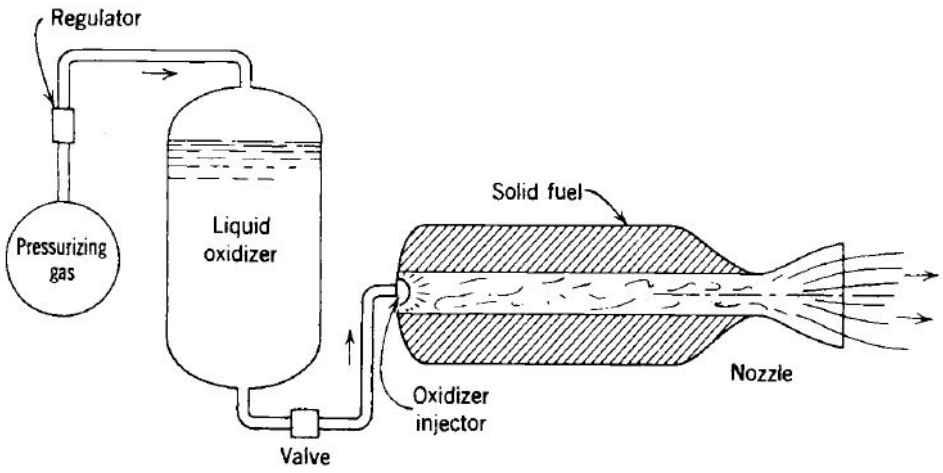

Figure 2.5: Classic scheme of a HRE, [30]

It can be seen that the liquid propellant is injected into a vaporisation chamber, upstream of the area occupied by the grain. This maximises combustion efficiency. There are several advantages to this solution, which can be summarised as follows:

- Active temperature control in the nozzle by having a liquid propellant;
- Thrust regulation as you have control over the flow rate of oxidant to the chamber. This is an advantage that is however limited by the fact that changing the flow rate necessarily changes the Mixture Ratio (MR). However, it is possible to insert part of the oxidant flow downstream of the grain, in the mixing zone, in order to bring the MR back to the expected values. In addition, as the oxidant flow rate can be adjusted, it is possible to re-ignite the entire propulsion system;
- Limited costs, similar to SRM: in fact, there are few extra elements compared to using only solid propellants;
- Very high safety levels as the two propellants are stowed in two separate containers.

Unfortunately, this solution has shortcomings, especially in terms of combustion efficiency and regression rate, which is an order of magnitude lower than SRM.

2.1.4 Hypergolic

A particular solution concerns hypergolic propellants. These are combinations of fuel and oxidants which, when placed in contact, react spontaneously and initiate combustion without the necessity of supplying them with a certain activation energy. Self-ignition thus eliminates the need for a complex ignition system, reducing the risk of failure and increasing the overall reliability of the propulsion system. In addition, they allow very simple system re-ignition, making them an excellent solution for space applications for attitude control as they are storable for long periods, without performance degradation, and immediately ready for use. Another classic example for which they are being used is as a thermal igniter in SRM. However, their performance is very limited and, in addition, most classical propellants, such as Unsymmetrical Dimethylhydrazine (UDMH), are highly toxic to humans and the environment.

2.2 Emissions overview

To address the global climate crisis, emission regulations have become increasingly stringent. Therefore, an essential tool for achieving environmental goals is the assessment of the chemicals emitted by space launchers during the entire ascent phase. The emissions generated during ascent and reaching orbit are highly dependent on the technology used and, in particular, the composition of the propellants that power it. This aspect is of primary importance in the current

historical moment: in fact, environmental impact has become a primary aspect, together with performance optimisation and economic sustainability. The table 2.1 shows the main emissions generated by each type of launcher. An important aspect that must be considered when talking about emissions generated by space launchers is the impact on the upper layers of the atmosphere. In fact, as can be seen in the figure 2.6, the time the launcher spends in the upper atmosphere is about two-thirds of the total.

Type	**Oxidizer**	**Fuel**	**Major Primary Emissions**	**Global atmospheric impacts identified**
Liquid	LOX (Oxigen)	LH2 (Hydrogen)	H2O, H2	Cloud formation
	LOX (Oxigen)	RP-1 (Kerosene)	H2O, CO2, CO, H2	Ozone depletion Radiative forcing Cloud formation
	LOX (Oxigen)	CH4 (Methane)	H2O, CO2, CO, H2	Ozone depletion Radiative forcing Cloud formation
Solid	NH4ClO4 (Ammonium Perchlorate)	Al (Aluminium) & HTPB or PBAN	Al2O3, CO, HCl, H2O, N2, CO2, H2, Cl, NOx	Ozone deplation Radiative forcing Cloud formation
Hypergolic	N2O4 (Nitrogen Tetroxide)	N2H4 (Hydrazine), MMH or UDMH	N2, CO2, H2O, CO, NOx	Ozone depletion Radiative forcing Cloud formation
Hybrid	Liquid (e.g. N2O)	Solid (e.g. HTPB)	Varies	Varies

Table 2.1: Major primary emissions species for common rocket propellants and their environmental impact, [14, 28]

Although they are only a small fraction of the human-generated emissions in the atmosphere, they are the only anthropogenic sources of pollution above the troposphere, the impact of which needs to be investigated with particular attention.

It is important to know and understand the emissions because space traffic, and in particular space tourism, is growing strongly. Therefore, it is important to investigate, both locally and globally, the interaction that these emissions have with the surrounding atmosphere: in fact, considering the same particles can have very different repercussions from those usually found at sea level. In this sense, one example is water vapour. Although it is harmless in the troposphere, its impact is much greater at high altitudes. It contributes to the formation of clouds in the stratosphere and mesosphere, an area in which these are limited [33]. A classic

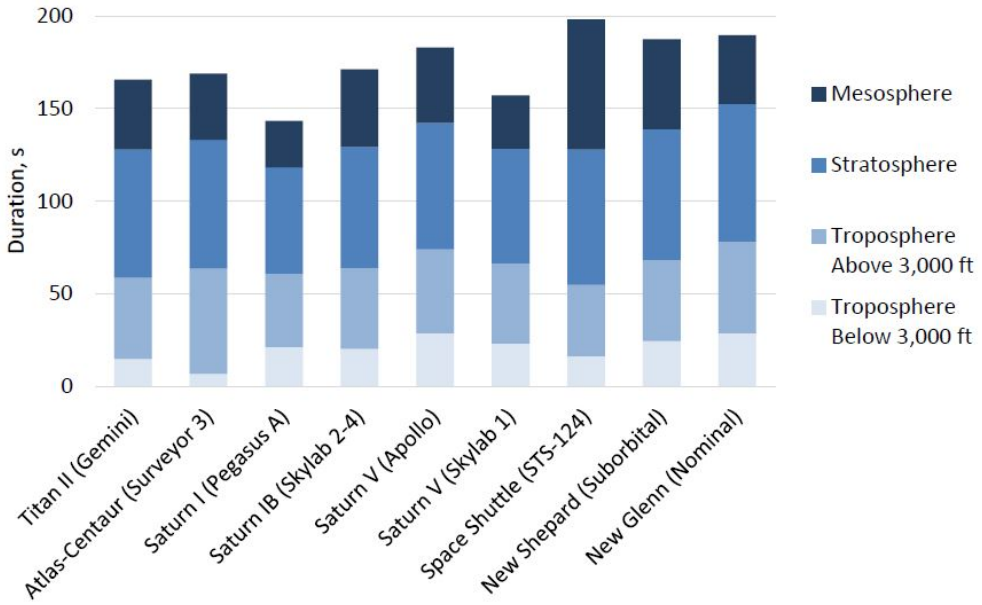

Figure 2.6: Time duration in each altitude band for historical and publicly available trajectories, [14]

solution adopted in the second stages of space launches is the combination of liquid hydrogen and liquid oxygen (LOX/LH2), which provide the highest performance in liquid propulsion. The combination of these two propellants, net of unburnt fuel, generates only water vapour, which is released into the upper layers of the atmosphere. In the case of the space shuttle, a 10-20% increase in the mass of mesospheric clouds in the polar region was observed following a single launch [16]. A further aspect of the atmosphere that is affected by launcher emissions appears to be the alteration of the ozone layer. The ozone layer is the region of the Earth's stratosphere that absorbs most of the ultraviolet radiation from the Sun, preventing it from reaching the ground. Its depletion is caused by its interaction with atoms and molecules that are present in the exhaust gases of space launchers. In particular, ozone reacts with molecules such as nitrogen oxides (NO_x), water, chlorides (CL_x), bromides (BR_x) and hydroxyl groups (OH), as well as chlorine-fluorocarbons [7]. According to these studies, the thinning was found to be a local effect: in fact, these elements act directly along the traversed ozone layer of the launcher's ascent trajectory. An explanatory example is the Delta II launcher, which uses oxygen and kerosene, causing a 70-100% destruction of the ozone layer in the vicinity of its combustion plume for about forty minutes, while the ARIANE 5 can affect this layer for up to four days [28]. The last aspect to be analysed, but no less important in its repercussions, is the environmental impact and climate change that these emissions

induce. Black Carbon (BC) is emitted by kerosene-fuelled engines and is generated in the case of incomplete combustion, while SRM also emits alumina particles, and both have the potential to cause positive Radiative Forcing (RF). RF refers to the alteration in the earth's energy balance. Specifically, a positive forcing induces a warming of the earth's surface and vice versa. An accumulation of BC and alumina in the stratosphere may absorb part of the solar flux, resulting in cooling of the Earth's atmosphere, but it will also trap the Earth's longwave radiation that would otherwise be scattered into space, resulting in warming [25]. Within the same study, it was found that the LOX/LH2 combination has the least impact on the Earth's energy balance as it does not produce any of the molecules that cause the highest effects, but, as already highlighted, only produces water vapour, which is found to have the lowest instantaneous RF of all, although not zero. An analysis carried out considering a total of one thousand annual launches with hydrocarbon-powered aircraft revealed that the cumulative effect of BC emissions generated over a decade would equal the radiative forcing generated by civil aviation [24]. A cascade effect would then be generated, leading to further depletion of the ozone layer caused by warming of the stratosphere. In the figure 2.7, it is possible to see the subdivision of the atmosphere and the molecules that have the greatest impact on it, and the repercussions generated by these molecules.

2.3 Emission estimation methods

The aim of this section is to present the methods known in the literature for estimating emissions in space launchers. One of the best known, and the basis for many other models, is the Chemical Equilibrium with Application (CEA) developed by National Aeronautics and Space Administration (NASA) [1]. It is a software that can analyse and solve various problems, including those related to combustion in launchers and rockets. By providing some basic data as input, the software is able to simulate the combustion analysis and provide as output the performance of the engine analysed, the thermodynamic properties at the various internal stations and at the interface with the external environment, and the chemical composition, expressed in mass fractions, at the end of combustion, i.e. when chemical equilibrium is reached. The greatest limitation of this software resides precisely in this last aspect: it assumes that combustion is a succession of chemical equilibrium states. This assumption makes the software incapable of obtaining compounds such as black carbon, which are generated under non-equilibrium conditions and non-homogeneous mixing. Furthermore, this software does not consider the interactions between the high-energy, high-temperature wake and the external atmosphere. A solution for this shortcoming has been implemented in the RUMBLE 3.0 software [13], a spatial version of the well-known tool adopted

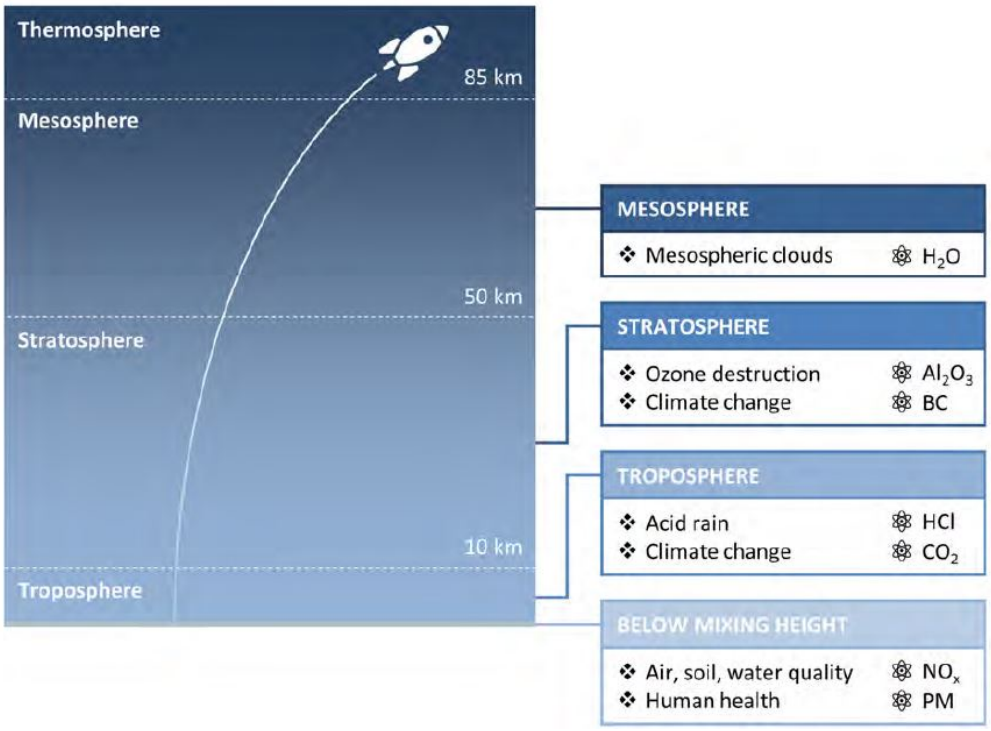

Figure 2.7: Examples of the environmental impacts of rocket emissions in each atmospheric layer and the important pollutants that determine those impacts, [14]

by the US civil aviation Aviation Environmental Design Tool (AEDT) [14]: in the article, primary emissions are referred to those generated in the combustion chamber and in the nozzle expansion phase before interaction with the atmosphere, which are assumed to be equal to those provided by the CEA. Secondary emissions are also considered to be the results of the interaction of the primary emissions, contained in the high-energy plume, with the surrounding atmosphere. However, these secondary emissions are obtained by considering emission indices (EIs) obtained through experimental fitting with data from the literature. This approach, although useful, is limited in two respects: it is necessary to have very reliable data available in order to obtain results that adhere to reality. In addition, this approach is only applicable to launchers using technologies similar to those used by the launchers used to generate the indices. Alternatively, the analysis of a space launcher's emissions can be carried out using high-fidelity simulations. These turn out to be the most reliable and accurate, but require an amount of information that is not available at the conceptual stage, and in the early stages of design. Based on what was presented previously, it can be seen that the current literature is very limited in methodologies for estimating emissions in the context of space

launchers. In order to limit these shortcomings, one possible approach could be to extend the methodologies for estimating emissions in the aviation field to the space sector. In particular, new formulations should be derived by considering both flight altitude and the chemical composition of the atmosphere since, compared to the troposphere, which is practically constant in composition, several variations can be observed, especially at high altitudes. In order to better understand what has been suggested, the main methodologies used in the aviation sector are presented below. It refers in particular to nitrogen oxides due to the fact that the atmosphere is mainly composed of nitrogen molecules. The schematisation of these methodologies can be seen in the figure 2.8.

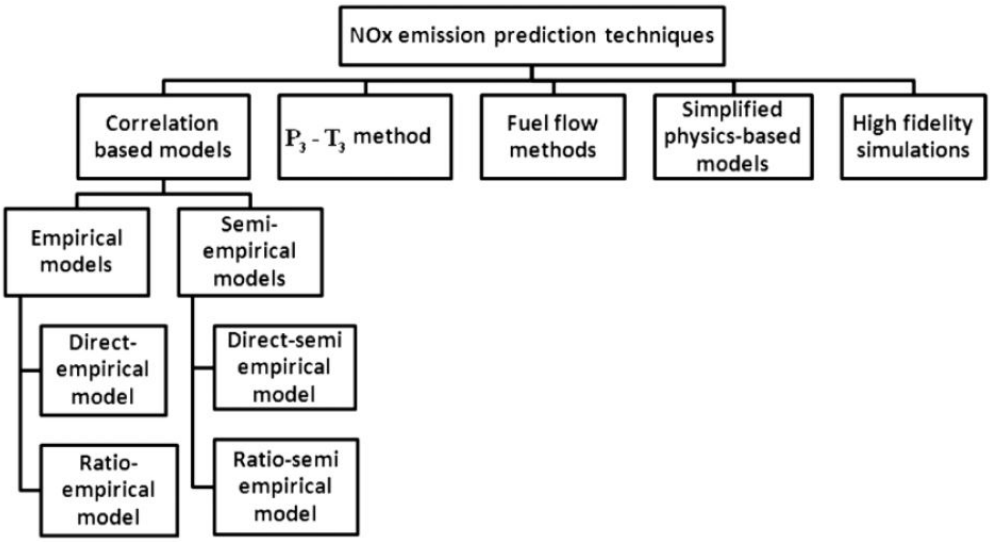

Figure 2.8: Classification of prediction methods for the estimation of NO_x emissions, [5]

2.3.1 Correlation-Based models

Correlation-based models are based on thermodynamic and emission data from engine tests under ground-level conditions. These data are integrated within mathematical formulations to determine the $EINO_x$ based on combinations resulting from analysing the correlations between these data and NO_x formation within the engine. These methods fall into two categories, empirical and semi-empirical, depending on the type of variables included in the final mathematical formulations. Specifically, the variables that characterise an empirical method based on correlations are the engine's primary parameters, such as combustion chamber inlet temperatures and pressures, combustion end temperature, Fuel-to-Air Ratio

(FAR) or water-to-fuel ratio (WFR). Semi-empirical methods, on the other hand, require detailed knowledge of the combustion chamber configuration and involve the use of combustor-specific variables, such as primary zone temperature, flame temperature, combustor volume and chamber residence time. Correlation-based models are further classified into direct models and ratio models. Direct models directly use engine parameters to estimate NO_x emissions, while ratio models express input variables as ratios between their values at flight level and standard sea level conditions (SLS). These methods offer the advantage of a wide range of variables to be analysed when generating mathematical formulations to estimate $EINO_x$, and some of these variables are easily estimated or readily available. Consequently, they are recognised as one of the most easily applicable types of methods in conceptual design. The downside is that in order to achieve acceptable accuracy in estimations with these methods, a considerable number of variables must be used. Each variable is subject to errors in detection or estimation, resulting in an accumulation of errors that becomes more significant as the number of variables considered increases. Despite being the simplest to apply, correlation-based models require a large amount of input data, which can be difficult to obtain, especially in the conceptual design phase. Derived exponents for some terms in the formulations may amplify the inherent errors in the input data. This constraint limits the models' ability to predict changes in NO_x emissions due to design changes, which can only be accurately assessed through physical testing of the engine. Finally, since correlation-based models are developed from experimental data specific to one engine, they cannot be generalised to other engines without significant adaptation. Although a fitting method exists, it must be repeated for each engine considered. This high degree of specialisation further limits the generalisability of correlation-based methods between different aircraft or engine designs.

2.3.2 $P_3 - T_3$ method

Of the simple prediction methods, the most dependable and popular one is the $P_3 - T_3$ method. In the aforementioned methodology, Emission Index (EI) at ground level is adjusted to align with the conditions present at altitude. This is achieved by utilising both altitude data and the operational parameters of the ground-level combustor. In contrast to the correlation methods previously described, the $P_3 - T_3$ method can be applied to all engines, with the same values of the exponent m and n being used. Nevertheless, should greater precision be required, engine-specific values of the exponents are employed. The $P_3 - T_3$ method is the most frequently employed approach for estimating NO_x emission indices. This method is derived from correlation-based models and focuses on a limited range of parameters of interest, including the inlet temperature and pressure to the combustor (P3, T3) and the FAR. These variables are included in the compact

mathematical formulation provided below:

$$EINO_{FL} = EINO_{SL} \left(\frac{p_{3,FL}}{p_{3,SL}}\right)^{n} \left(\frac{FAR_{3,FL}}{FAR_{3,SL}}\right)^{m} \exp(H) \tag{2.1}$$

$$H = 19 \cdot (h_{SL} - h_{FL})$$

where H is the humidity factor, which is introduced to account for the influence of humidity on NO_x formation in the combustion chamber. As this factor increases, the combustion temperature decreases, which leads to a reduction in NO_x production. The value of the H factor can be calculated based on the relative increase in specific humidity (h), expressed as $[kg_{H_2O}/kg_{dry\,air}]$, due to an increase in altitude. While the inlet temperature to the combustor, T_3, is not explicitly incorporated into the mathematical formulation, it plays a significant indirect role by influencing the applicability of the method and representing the determining parameter. Below the steps required to obtain $EINO_x$ estimates using this method are presented in [5]:

- The initial stage of the process requires access to specific proprietary engine data, provided directly by the manufacturer, rather than estimated through propulsion modelling. This data corresponds to the four throttle conditions prescribed in the International Civil Aviation Organization (ICAO) database for the Landing Take-Off (LTO) cycle. The data set comprises pressure and temperature at the combustor inlet ($p_{3,SL}$, $T_{3,SL}$) and FAR_{SL}, all evaluated under standard sea level conditions. In addition to the aforementioned propulsion data, it is essential to have access to $EINO_{x,SL}$ emissions data, which can also be obtained from the ICAO databank rather than estimated using dedicated software. Subsequently, the parameters $p_{3,SL}$, FAR_{SL}, and $EINO_{x,SL}$ must be plotted as functions of T_3 and appropriately interpolated in order to obtain an optimal fit;

- Once the fits have been generated in sea-level conditions, the next stage is to derive the values of the aforementioned parameters under flight level conditions: these are $p_{3,FL}$, $T_{3,FL}$ and FAR_{FL}. As previously stated, this information should be obtained directly from the engine manufacturer rather than through propulsion modelling;

- From the values of $T_{3,FL}$ obtained in the preceding step, it is possible to deduce the parameters $EINO_{x,SL}$, $p_{3,SL}$, and FAR_{SL} using the fits obtained in the initial step. Once the parameters have been identified, the next step is to construct ratios that relate flight and sea level conditions. This is because the $P_3 - T_3$ method is based on a ratio approach, and these ratios are embedded in the method's underlying mathematical formulation;

- Ultimately, the mathematical formulation of the method mentioned above can be employed to assess the $EINO_{x,FL}$, beginning with the appropriately adjusted $EINO_{x,SL}$ and considering the evolution ratio of p_3, FAR, and the humidity factor. It has been demonstrated that the best results are obtained when using exponential coefficients m and n, where n=0.4 and m=0. This methodology, however, also permits the utilisation of enhanced coefficients for a given case study, thereby facilitating the attainment of more precise results.

2.3.3 Fuel flow methods

The fuel flow method is a method of estimating NO_x emissions generated from $P_3 - T_3$ but in a form that does not have to take into account proprietary data that may not be available. This is a more simplified approach that may affect the accuracy of the results obtained. Several exist in the literature, but in this section we refer to the most common, namely the Boeing Fuel Flow Method 2 (BFFM2). In this case too, the emission indices at altitude are derived, by means of direct correlation, from those obtained on the ground. The parameter on which this method focuses most, as can be guessed from its name, is the fuel flow, which is conceptually comparable to the engine's thrust condition. In addition to this, the method considers both flight and environmental conditions as input parameters: in particular, the flight mach (M), humidity factor (H), temperature and ambient pressure are considered. The flight mach is necessary in able to derive, by means of the correlation 2.2, the fuel input to the ground corresponding to the consumption at altitude. This newly calculated parameter does not result directly in the calculation of the $EINO_{x,FL}$ but is used to obtain, by interpolation of the data, the $EINO_{x,SL}$ which are then used to derive those at altitude, as can be seen in the 2.3. Below are the steps required to calculate the emission indices according to BFFM2:

- The first step involves calculating the flow rate of fuel consumed on the ground corresponding to the flow rate consumed at altitude and as a function of all other parameters considered:

$$W_{f,SL} = W_{f,FL} \frac{\theta_{amb}^{a}}{\delta_{amb}^{b}} \cdot \exp\left(c \cdot M^2\right) \tag{2.2}$$

$$\theta_{amb} = T_{amb}[K]/288.15$$

$$\delta_{amb} = p_{amb}[Pa]/101325$$

  Exponents specifically derived for a particular condition can be used or those presented by the original formulation can be used: a=3.8, b=1 and c=0.2.

- The $EINO_{x,SL}$ obtained from the ICAO database are now interpolated as a function of the corrected fuel flow rate under sea level (SL) conditions obtained earlier;
- The $EINO_{x,FL}$ corresponding to the fuel flow conditions obtained in step 1 are now derived using the following formulation:

$$EINO_{x,FL} = EINO_{x,SL} \left(\frac{\theta_{amb}^{d}}{\delta_{amb}^{e}} \right) \exp\left(H\right) \tag{2.3}$$

  Again, it is possible to use exponents derived for the specific case or to use those provided by the original method which are: d=1.02, e=3.3 and f=0.5.

2.3.4 Simplified physics-based models

In order to achieve a deeper understanding of the combustion process, simplified physics-based models have been developed that outline the combustion process from a physical perspective. These models involve dividing the combustion chamber into discrete regions, each characterised by distinct assumptions and concentrations of specific species. Subsequently, the combustor is modelled as a network of multiple ideal reactors, each of which is suitably simplified according to the governing assumptions of the respective region. This approach reduces the computational cost associated with simulating the combustor in its entirety. However, these models are unable to accurately represent the complex kinetic processes involved in pollutant formation, which limits their suitability for use in hydrogen-powered aircraft applications.

2.3.5 High Fidelity Simulation

High-fidelity simulations prove to be the most accurate model for calculating and estimating emissions. However, as already mentioned, they require a range of data that are not yet available in the conceptual stages of design. In particular, it is necessary to know the geometry of the combustor, the kinetics of NO_x formation and the thermodynamic quantities of the combustion chamber. Speaking of high-fidelity analysis, it refers to the use of Computational Fluid Dynamics (CFD) tools. The most widely used are:

- Reynolds-averaged Navier-Stokes (RANS), which can only be applied if the boundary conditions in the combustor are known;
- Direct Numerical Simulations (DNS), which are the most suitable as they are able to describe complex combustion phenomena but are highly inefficient from a computational point of view;

- Large EDDY simulations (LES), which implement small-scale turbulence models for combustion processes. Although the accuracy of this solution is lower than the previous one, they are still simulations that require a high computational cost.

Consequently, all the solutions presented are not applicable at the conceptual design stage due to their high computational costs and the fact that they require details that are not yet known at this stage of the design. Therefore, these analyses are usually employed in the subsequent design phases, when detailed analyses are carried out.

Chapter 3

Case study

This brief chapter analyzes the Synergetic Air-Breathing Rocket Engine (SABRE), the propulsion system under development at Reaction Engines Limited (REL), which has been used as a case study for developing the model and applying the proposed methodology for estimating emissions in rockets.

3.1 Skylon

Before introducing the SABRE, a brief overview is given of the Skylon, the aircraft utilizing this engine as its propulsion system. Skylon is a fully reusable Single-Stage-To-Orbit (SSTO) under development at REL since 2009. This particular vehicle will be capable of taking off and landing like a conventional aircraft, thus falling into the category of Horizontal Take-Off Landing (HTOL) vehicles. The advantages provided by this type of vehicle are numerous and significant. In particular, ground operations are considerably simplified compared to traditional launchers that require transport by other means. Skylon will be autonomous on the ground and can be prepared for flight in a hangar, avoiding the costly logistical challenges associated with traditional launch facilities. This spaceplane is designed to Low Earth Orbit (LEO) orbit with the aid of two SABRE engines onboard. These engines cover the entire mission profile through their two operational modes: initially, Skylon takes off from an extended runway using its engines in air-breathing mode, accelerating to Mach 5.14 and reaching an altitude of 28.5 km. At this point, it switches to rocket mode to propel the vehicle to the required mission altitudes. This approach allows the vehicle to utilize atmospheric oxygen for fuel oxidation during the initial stages, significantly improving the Mass Ratio to approximately 23%, roughly double that of a conventional launcher [10]. Once the ascent and orbital insertion are completed, Skylon will proceed to open its cargo bay and allow deployment of the onboard payload. The descent phase begins from an altitude

of 120 km. During this phase, the vehicle maneuvers to manage heat flows and thermal loads, adhering to predefined requirements necessary to return to the designated spaceport for landing. Following a gliding approach similar to the Space Shuttle, it reaches the landing runway.

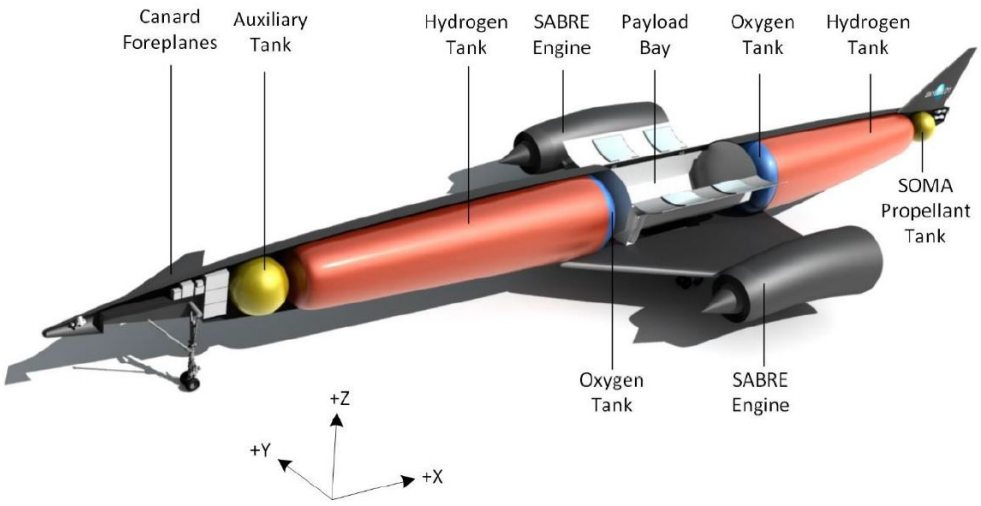

Figure 3.1: Skylon layout, [10]

As can be seen in figure 3.1, the central body of Skylon features a slender fuselage designed to house cryogenic propellant tanks and a top-accessible cargo bay. There is a clear separation between the fuselage and the delta wings positioned approximately halfway along the airframe. Although this solution appears to be the best in terms of optimising volume, lift and weight, it is critical in several respects: in particular, the solution adopted makes it complicated to manage the thermal loads that develop in the wing-fuselage interaction zone and on the leading edge of the wings. To overcome this, the use of active cooling systems is necessary. Another critical aspect of this solution is the interaction of the engine trails with the fuselage. In fact, the low atmospheric pressures at high altitudes mean that the combustion wake can expand and directly affect the end of the fuselage [18]. At the wingtips, the two SABRE engines are mounted using an axially symmetric nacelle. A notable aspect of the SABRE nacelle is its curved shape, which is necessary because, especially at low speeds when Skylon's mass is greater due to full tanks, the wing's angle of attack must be high. However, it is crucial that the incoming airflow remains parallel to the intake for shock symmetry. This alignment cannot be achieved with engines fixed at a set angle relative to the vehicle, as it would cause misaligned thrust, especially during rocket phases. Therefore, a curved nacelle design is adopted to allow for better airflow entry angles while ensuring the exhaust remains aligned with the fuselage to minimize misalignment losses. The

primary characteristics of Skylon in terms of mass and dimensions are detailed in Table 3.1.

Fusolage lenght	83.1 m
Wing Span	26.8 m
Height	13.5 m
Max Payload Mass	15.0 tons
Gross Take-Off Mass	325.0 tons
Dry Mass	53.4 tons
Usable Ascent Propellant	250.1 tons
Initial Mass of Rocket Phase	300 tons

Table 3.1: Dimensional and mass characteristics of the Skylon spaceplane, [10]

The central body, excluding the cargo bay, is primarily occupied by liquid hydrogen tanks. This allocation is facilitated by the fact that, during the initial ascent phase, the oxidizer is sourced from external air, and hydrogen's low density necessitates larger fuel tanks. In addition to the primary tanks, there is the Skylon Orbital Manoeuvring Assembly (SOMA) tank, which houses the propulsion module for orbital maneuvers. The tanks are strategically divided to balance the vehicle's weight distribution. Skylon features control surfaces for atmospheric flight, including Canard foreplanes for pitch control, ailerons for roll control, and an aft fin for yaw control. During the pure rocket phase, control relies on differential engine thrust.
Regarding materials, the primary structure comprises a frame of titanium struts reinforced with silicon carbide, while the aluminum tanks are suspended using Kevlar ties. The frame is covered with sheets of reinforced glass ceramic material, serving as both the aeroshell and the primary thermal protection system, complemented by a multilayer metallic heat shield. In Figure 3.2 and 3.3, a typical ascent and descent trajectory considered by REL for Skylon can be observed.

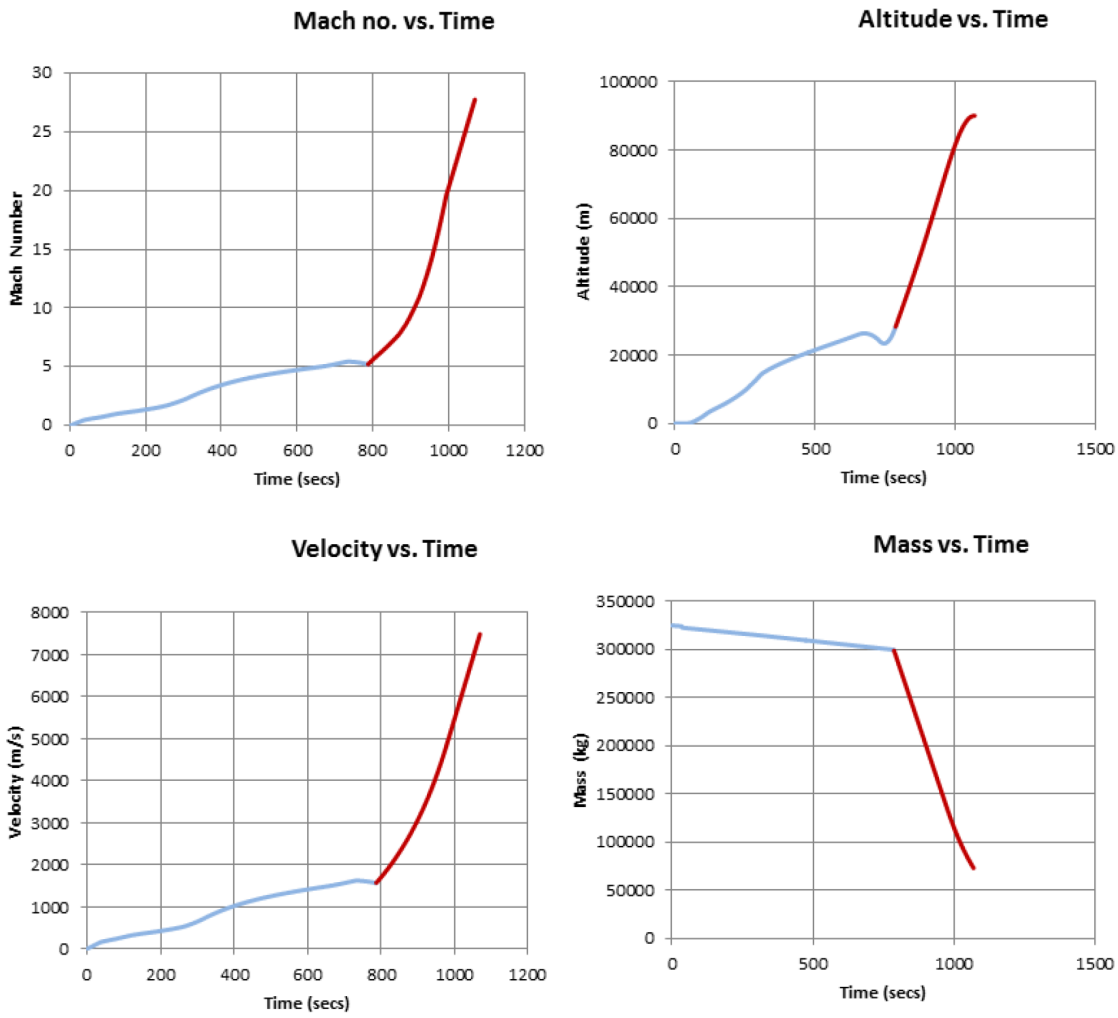

Figure 3.2: Ascent trajectory, [10]

3.2 SABRE Engine

The SABRE is the key component of the Skylon, enabling the single-stage-to-orbit vehicle to operate in both air-breathing and rocket modes. If Skylon can be considered as the evolution of the British Aerospace HOTOL, then SABRE represents the evolution of the Liquid Air Cycle Engine (LACE), which eliminates the need for air liquefaction, a significant challenge in the previous design. This unique engine concept operates like a turbojet, utilizing hydrogen as fuel in combination with air from take-off until the transition point, set at an altitude of 25 km, enabling the engine to reach a Mach number of 5. Once this speed regime is reached, the

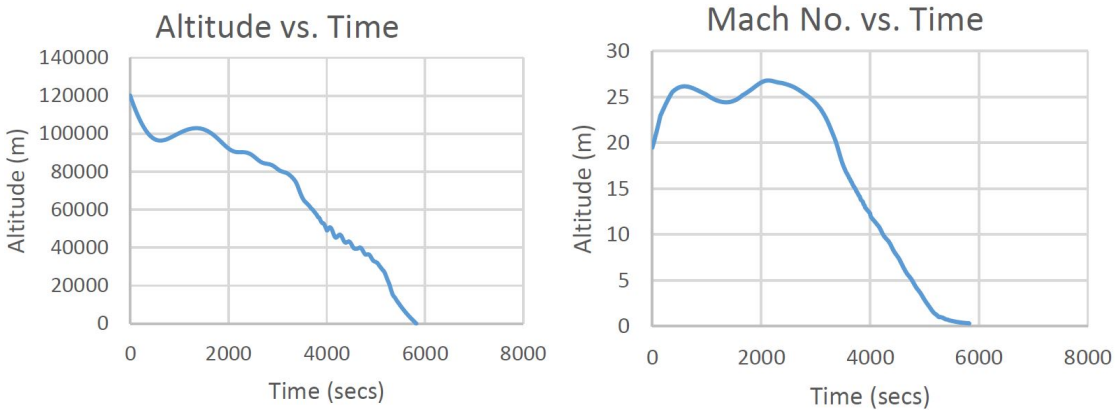

Figure 3.3: Descent trajectory, [10]

engine transitions to rocket mode, during which air is replaced by Liquid Oxygen (LOX), ensuring a specific energy release during combustion compatible with the levels required for ascent to low Earth orbit. The transition of the the SABRE to rocket mode occurs at an altitude where it is no longer feasible to sustain Liquid Hydrogen (LH2)-external air combustion due to the rarefied conditions of the atmosphere at that altitude. However, this innovative engine allows to keep together the advantages of air breathing and rocket engines, as the air-breathing operating mode allows for a reduction in the amount of propellant needed to be stored inside the Skylon to ensure access to the target orbit, consequently increasing the payload mass that can be transported to its destination, while the engine in rocket mode provides high delivered thrust. In addition, according to [8], in the first phase of flight, in an exoreactor-like configuration, the emissivity of the engine is much lower than in classic rocket solutions such as Space Shuttle and Falcon 9. The architecture of the the SABRE is well summarized by Figure 3.4 provided by V. Fernandez Villacé [32] and, as it can be seen, it is a turbomachinery-based cycle for the air-breathing phase, allowing the generation of static thrust, differently from a ramjet or a scramjet.

Regarding its air-breathing operating mode, the SABRE falls into the category of deeply precooled combined cycle engines, where the primary air cycle is coupled with a secondary regenerative cycle using helium for thermal management of the engine. The critical component that enables the significant cooling of the inlet flow to the engine is the Pre-Cooler (PC), which is the subject of extensive research by REL.

As can be seen in figure 3.5, it consists of a series of adjacent microchannels through which helium flows, allowing the incoming flow to be cooled from 1200 K to 100 K. The low temperatures at the compressor inlet enable very high compression

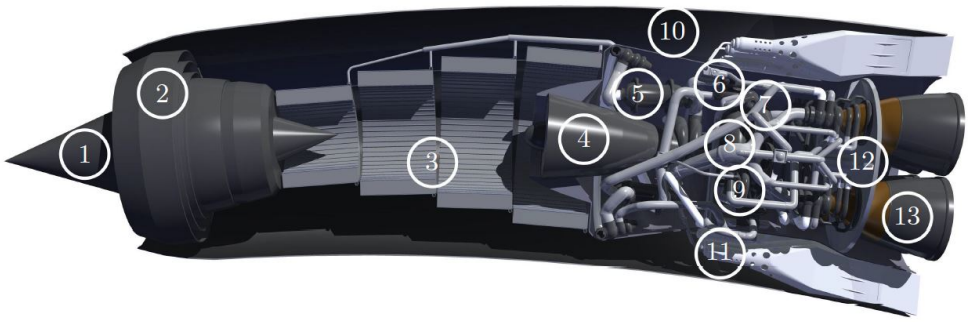

Figure 3.4: SABRE section: 1) movable spike 2) intake 3) precooler (PC) 4) air compressor (AC) 5) pre-burner (PB) and reheater (HX3) 6) helium circulator 7) H2 pump 8) He turbine and regenerator (HX4) 9) LOx pump 10) spill duct 11) ramjet burners 12) heat shield 13) thrust chamber, [32]

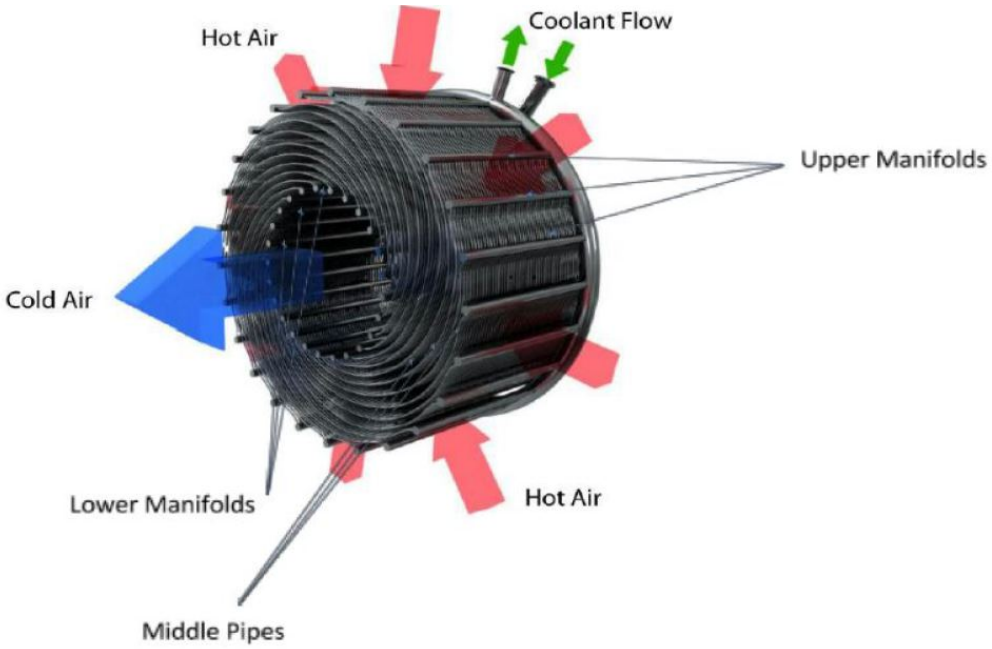

Figure 3.5: Pre-cooler design. [15]

ratios that would otherwise be unattainable due to the technological limits of the materials constituting the compressor. There are many issues associated with this component, the most significant being ice formation, which would disrupt the flow entering the compressor and adversely affect the engine's performance. The use of helium as heat sink allows for the regeneration of a portion of the heat extracted from the hot incoming airflow into the engine, extending its operation

in air-breathing mode up to a Mach regime exceeding 5 without performance degradation, particularly in specific impulse. Additionally, the SABRE involves a two-stage combustion process occurring in two different combustion chambers: the Pre-Burner (PB) and the main Combustion Chamber (CC), enabling the regeneration of a portion of the heat produced during the initial combustion segment, again utilizing the helium cycle. The regenerated heat through the helium cycle is utilized to heat the cold flow of hydrogen stored at a temperature close to 0K to maintain its liquid state during storage, as well as to power the compressor involved in the primary air cycle. As reported in V. F. Villàcé [32], the incoming air captured by the intake is deeply cooled inside the PC, then passes through the high-pressure ratio Air-Compressor (AC), downstream of which the flow is split with a variable splitting ratio depending on the flight Mach number and redirected to the two combustion chambers. The two-stage combustion takes place first in the PB, where a portion of the air is burned under fuel-rich conditions. The exhaust gases from the PB, after exchanging some of their heat in the Heat Exchanger (HX)3 with helium, rejoin with the second airflow from the splitting at the main CC, where combustion is completed again under fuel-rich conditions. Finally, the combustion products from the main CC expand in the nozzle, generating thrust. Additionally, since the nacelle and the air intake are designed to operate at an altitude of 25 km, a ring of ramjet burners has been introduced To manage the excess air flow rate. At altitudes below the design altitude, it is necessary to manage the straight shock wave generated in the throat of the air intake by bleeding off a certain flow rate, which is then directed to the bypass burners along with a small fraction of fuel. This prevents the generation of significant drag and the associated loss of performance and efficiency that would occur if part of the intake airflow were not utilized. Regarding the engine operation in rocket mode, the engine cycles are shorter as the air intake is closed, and the two-stage hydrogen-air combustion is replaced by a single stage of hydrogen-oxygen combustion. Oxygen in this configuration contributes to heat regeneration by cooling the walls of the main chamber combustion, thereby recovering some of the heat produced during the hydrogen combustion. Since the helium no longer has access to the energy and heat provided by the PC and HX3, it is energized using the heat released during the exhaust gas expulsion in the nozzle. Specifically, the helium is used to cool the walls of the nozzle. As reported in the Skylon User Manual [10], this engine can provide a gross thrust of approximately 2 MN per nacelle in both of its operating modes. In the air-breathing phase, it offers a specific impulse ranging from 40,000 to 90,000 [Ns/kg]. However, in the rocket phase, the specific impulse value is around 4500 [Ns/kg]. The architecture of the SABRE engine is indeed custom-designed for space access, offering significant advantages. It provides a high thrust-to-weight ratio during air-breathing operation, coupled with moderate specific fuel consumption, which enables efficient propulsion during the initial phase

of flight. Furthermore, as it transitions to rocket mode, it maintains a high specific impulse, ensuring optimal performance during the phase of reaching the target orbit. Table 3.2 summarises the SABRE performance.

Mode	**Air-Breathing**	**Rocket**
Altitude Range [km]	0 - 28	28 - 90
Mach No. Range	0 - 5.5	5.5 - 27.8
Approximate Gross Thrust ([MN], per nacelle)	0.8 - 2	2
Approximate Specific Impulse [s]	4000 - 9000	450

Table 3.2: SABRE performances, [10]

The most up-to-date version of the model of SABRE in the air-breathing mode, proposed by Grimaldi [9], is shown in figure 3.6. This modelling will be used as a reference for the realisation of the model of SABRE in rocket mode.

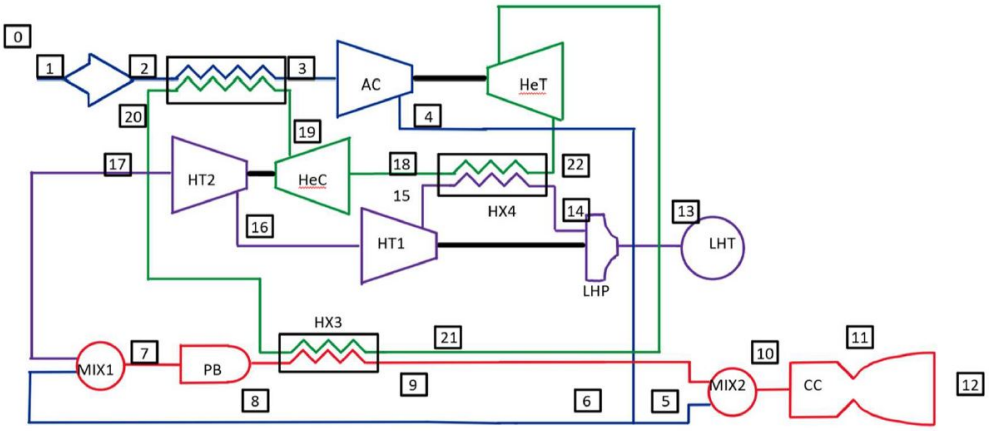

Figure 3.6: Model of SABRE in air-breathing mode, [9]

Chapter 4

Hydrogen

Before proceeding with the modelling of the rocket mode of the Synergetic Air-Breathing Rocket Engine (SABRE), we want to study hydrogen and its combustion, in order to understand the reasons for this choice of propellant in the Skylon's power supply. The interest that hydrogen has as a propellant is linked both to a performance argument, as it is highly efficient in terms of thrust generation, but also to an environmental sustainability argument. The use of hydrogen as a fuel eliminates the formation of both Black Carbon (BC) and carbon oxides that are typical of hydrocarbon combustion. This generates significant benefits in terms of limiting Greenhouse Gas (GHG) emissions. In fact, hydrogen has a Global Warming Potentials (GWP) value that is orders of magnitude smaller than that of CO2. However, it is not possible to reduce the impact of aviation and space launches to carbon dioxide emissions alone: in fact, as already mentioned, there are several elements that can have an impact on the atmosphere and its layers. Therefore, it is important to study the role that hydrogen plays in the formation of these molecules. Before proceeding, the intrinsic properties of hydrogen are presented. Lately, thanks to projects such as *MORE&LESS*, efforts are being made to make hydrogen an alternative to the classical fuels used in high-speed and long-distance aviation. One aspect to be analysed is the physical state in which hydrogen is found when used as a propellant. In fact, its liquid form is preferred over its gaseous form. This is because it has a much higher energy density, which in aerospace applications is fundamental in that better performance and efficiency can be achieved. This is about 2.5 times higher than that of a fossil fuel, which means that less of it can be used, even though, due to its low density, the volumes occupied are very high. Moreover, it is an excellent coolant, being liquid and cryogenic, and allows active management of the heat generated in certain critical phases of flight and in certain localised areas, such as the exhaust nozzle or aerodynamic surfaces subject to shock waves. A further advantage comes from a physical and chemical point of view, as hydrogen can be assumed to be an ideal gas over a very high

temperature range and even at high pressures. The table 4.1 summarises the main characteristics of hydrogen. It should be noted that the range of flammability in air varies from 4% to 74% [27]. Furthermore, the auto-ignition temperature is higher than that of a fossil fuel, so it makes it possible to operate at higher pressures and temperatures safely and further increases combustion efficiency. However, it may require the introduction of an igniter to allow the mixture to ignite.

Parameter	**Hydrogen**
Molecular weight [g/mol]	2.01588
Boiling point @ P = 1 atm [K]	20.268
Melting point @ P = 1 atm [K]	14.01
Density of gas @ STP [kg/m^3]	0.08990
Flammability limits in air [vol %]	4.0 - 75.0
Auto-ignition temperature in air @ 1 atm [K]	793 - 1023

Table 4.1: Hydrogen properties, [27]

4.1 Hydrogen Combustion

Although SABRE in rocket mode combines Liquid Oxygen (LOX) and Liquid Hydrogen (LH2) producing only water vapour, it is necessary to consider what happens in the wake, where the hot gases, also containing some unburned fuel, interact with the surrounding atmosphere. As mentioned earlier, hydrogen combustion is significantly less impactful than fossil fuels, but its emissions are not negligible. In fact, although emissions such as carbon oxides are eliminated, water vapour and nitrogen oxides are still generated due to interaction with the air. In particular, the main nitrogen oxide produced by combustion is NO, while oxides such as NO_2 are produced in significantly smaller quantities. Below is a brief presentation of the emissions generated by air/hydrogen combustion.

4.1.1 Water vapour

As previously established, this gas is harmless and non-impactful within the troposphere, as is the case with all classical aviation, as it falls back to the ground very quickly due to meteorological phenomena. However, at higher altitudes, this argument is no longer valid. In fact, water vapour has been shown to be a greenhouse gas and, due to its durability of up to several years [35], has a huge impact in terms of Radiative Forcing (RF), especially in the stratosphere. Furthermore, it is a catalyst to the ozone layer and its impact is even greater than that caused by nitrogen oxides [17]. The impact of these emissions is expected to increase in the coming years due to the adoption of the transition to hydrogen-powered aircraft. For this reason, water vapour emissions into the atmosphere are of primary concern.

4.1.2 Nitrogen Oxides emissions

The nitrogen oxides produced during hydrogen/air combustion are mainly composed of nitric oxide (NO), with all other oxides being a small part [12]. Nitrogen oxides are formed as a result of the interaction of molecular nitrogen in the air, which, due to the high temperatures reached in combustion, dissociates and, after a series of chain reactions, achieves a stable form in nitrogen oxides. These pollutants do not contribute directly to global warming, but generate a radiative effect through interaction with other molecules in the atmosphere. This is highly dependent on the exposure time, and the spatial position in which these molecules interact. The main effects these oxides cause concern the depletion of the ozone layer in the stratosphere and the reduction of ambient methane. The first mechanism is due to the fact that nitrogen monoxide acts as a catalyst for the breakdown of the ozone molecule, causing a positive RF. The interaction between these molecules causes the formation of hydroxyl radicals that tend to destroy the methane dispersed in the environment. This is a positive aspect as methane generates a positive RF. In the following, various mechanisms of nitrogen oxide formation are analysed. In particular, since we assume the $z24\_nox$ as the kinetic scheme for the analysis of internal combustion in SABRE and subsequently as the wake interaction with high-energy combustion gases, only those mechanisms predicted within it are analysed.

Thermal NO (Zeldovich mechanism)

Thermal NO, also known as Zeldovich NO, are formed by the following reactions:

$$N2 + O \rightarrow N + NO$$

$$N + O2 \rightarrow NO + O$$

$$N + OH \rightarrow H + NO$$

This mechanism is described as thermal because it only occurs at temperatures exceeding 1800K. In fact, the activation energy required to break the triple bond that binds an N_2 molecule is very high. When the temperature is below the threshold highlighted by Zeldovich [37], the formation reaction is so slow that the formation of nitrogen monoxide is unlikely to occur [34].

N/O sub-mechanism

This mechanism involves the formation of NO from other nitrogen oxides: in particular, four chemical species come into play, which are nitric oxide (NO), nitrogen dioxide (NO_2), nitrous oxide (N_2O) and finally nitrogen trioxide (NO_3). The latter is, however, of minor influence in this mechanism, which is why it is not present in the kinetic scheme used. The reactions contained within it that are linked to this mechanism can be observed below:

$$NO2 + M \rightarrow NO + O + M$$

$$H + NO2 \rightarrow NO + OH$$

$$N2O + O \rightarrow NO + O2$$

$$N2O + O \rightarrow 2\,NO$$

Within this mechanism, nitrogen monoxide plays a dual role: it is generated by recombination to eliminate free radicals, as it is a more stable molecule compared to the others in the chain. Otherwise, it acts as a chain carrier, stimulating further reactions with nitrogen compounds [38]. This mechanism is predominant at low temperature and high pressure: in fact, high pressure favours these reactions while low temperature is sufficient to break the weak bonds that make up the NO_2 and N_2O molecules.

H/N/O sub-mechanism

The H/N/O mechanism includes five chemical species, respectively called nitroxyl (HNO), HON, nitrous acid isomers ($HONO/HNO_2$) and nitic acid isomers ($HONO_2$) [38]. However, only reactions where nitroxyl is available are included in the kinetic scheme considered, as shown below:

$$H2O2 + N2 \rightarrow NH + NO + OH$$

$$NH + OH \rightarrow H + HNO$$

$$NH + O2 \rightarrow HNO + O$$

$$HNO + OH \rightarrow H2O + NO$$

$$H + HNO \rightarrow H2 + NO$$

This compound is generated from the intermediate species NH, which is generated during the combustion of hydrogen peroxide and molecular nitrogen. It should be noted that the chemistry governing this mechanism is still particularly unknown, especially at high temperatures.

4.2 Cantera Software

In the work of this thesis, the simulation of combustion between LH2 and LOX and the subsequent mixing between the high-energy combustion gases and the external environment is simulated using Cantera. This is an open source software for zero-dimensional chemical-mathematical modelling. In the context of this thesis, it was used in both its Python and Matlab interfaces, although the latter software was essentially used as a comparison in the calculation of thermodynamic properties at specific engine stations. Cantera is capable of evaluating chemical equilibrium conditions in the combustion chamber and performing zero-dimensional simulations in function of time. In particular, these simulations are performed on homogeneous, adiabatic, isochoric and isobaric reactors containing carefully premixed reactive gaseous mixtures of hydrogen and oxygen. In order to model the kinetic and thermodynamic evolution of the mixture, Cantera solves the mass and energy balance equations shown below:

$$m_{tot} = \sum_{k=1}^{K} m_k \; = \; const \iff \frac{dm_{tot}}{dt} \; = \; 0 \tag{4.1}$$

$$\frac{dm_k}{dt} \; = V \, r_k \, M_{w,k} \tag{4.2}$$

$$c_{p,mix} \frac{dT}{dt} \; + \; v \cdot \sum_{k=1}^{K} h_k \cdot r_k \cdot M_{w,k} \; = \; 0 \tag{4.3}$$

In particular, it can be seen that the equation 4.1 refers to the conservation of total mass, while the mass of the single compounds varies according to the equation 4.2. Lastly, the equation 4.3 governs heat exchanges. Since the mixing temperature is lower than the hydrogen auto-ignition temperature, the presence of an electric igniter inside the combustion chamber is required to provide enough energy to ignite the mixture. In particular, the parameters with which it was modelled are shown in the table 4.2.

The terms given represent:

- The thermal energy a, which is the energy supplied for the ignition;

a $[W/m^2]$	**b** [s]	τ [s]
$8 \cdot 10^7$	0.09	$1 \cdot 10^{-8}$

Table 4.2: Electric ignition parameters

- The pulse width b. This is the time interval within which energy is supplied to the mixture. In order to decrease the Ignition Delay Time (IDT), this value must be decreased so that the same energy is supplied in a shorter time interval.
- The time at which this energy pulse is supplied τ. This must be as short as possible in order to trigger the mixture at the start of the simulation.

To realise these time-dependent simulations of combustion, Cantera needs as input the thermodynamic properties of the mixture, such as pressure and temperature, and its composition, which can be expressed as molar or mass fractions or as Mixture Ratio (MR). In response, the software will provide, within a *.csv* (Comma Separated Values) format file, the time-history of combustion. This is a succession of non-equilibrium states representing the state of the mixture as it changes over time. From these files it is possible to extract some variables that are of particular interest for this study. In particular:

- The equilibrium temperature, which is obtained at very high times at which equilibrium can be considered to have been reached. This temperature corresponds to the Adiabatic Flame Temperature (AFT).
- The IDT, this is the time delay between the start of the simulation and the time by which the mixture is considered to be ignited. There are several methods by which this time can be derived. The most reliable is the mass fraction of OH radicals: IDT turns out to be equal to the simulation time at which the first peak in the concentration of these radicals is obtained.
- The mass composition of all species considered by the kinetic mechanism

These variables will be used in the following discussion to obtain the emission indices for nitrogen oxides (NO_x) and water vapour (H_20).

Chapter 5

Modeling of SABRE in rocket mode

This chapter aims to present the model developed to represent the Synergetic Air-Breathing Rocket Engine (SABRE) propulsion system in its rocket mode operation, which, according to Reaction Engines Limited (REL), extends from an altitude of 25 km and a flight Mach number of 5 to low Earth orbit. As there are no existing models of the SABRE in rocket mode in the literature, the model developed in this thesis was created based on the complete schematic for the air-breathing phase by Grimaldi [9], in figure 3.6, and the ideal rocket engine model. In addition, typical solutions adopted in space launchers were assumed for the completion of the model. In particular, the active refrigeration of the nozzle by one of the cryogenic fuels on board the spaceplane. In the figure 5.1, it is possible to observe the schematic of the model that was realised for the description of the SABRE in rocket mode.

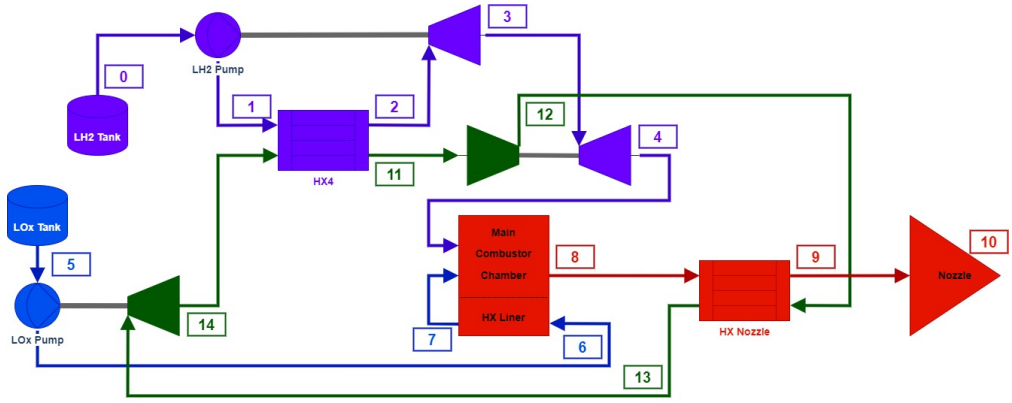

Figure 5.1: Modeling of SABRE engine in rocket mode

This modeling is simpler compared to the one used to describe the air-breathing mode because, after the transition from air-breathing mode to rocket mode, the air intake is closed, and both the precooler and compressor are bypassed. It is also important to note the absence of the pre-burner in this model, as it is unnecessary for maximizing thrust. In fact, the dual combustion chamber configuration is used in the air-breathing phase solely to provide additional energy to the helium cycle via the Heat Exchanger (HX) 3. Another difference from the previous model is the method of providing energy to the helium. In the air-breathing schematic, the helium absorbed heat from the precooler and the HX3. However, in the solution adopted in this thesis, the noble gas is regenerated through heat exchange in the nozzle, where it is used as a coolant for the walls, unlike classical launcher solutions where the coolant fluid is usually the fuel. In the table 5.1, the input data assumed for the implementation of the model of the SABRE in rocket mode are shown. It should be noted that all values that do not have a reference have been assumed within this discussion.

In this model, four different thermodynamic circuits can be identified: the hydrogen circuit (purple), the oxygen circuit (blue), the helium cycle (green), and the exhaust gas thermodynamic circuit (red). These are all open circuits, meaning there is no recirculation of matter and energy, except for the helium cycle, which is closed and thus requires the same initial and final conditions. This will be one of the constraints imposed during the modeling phase. The various circuits will be presented individually below, followed by an explanation of the individual stations indicated in figure 5.1 and their thermodynamic modeling, in order to make the model accessible to everyone.

5.1 Methodology

The capacity to estimate the emissions generated by the aerospace sector and, in this particular case, by space access systems, has become crucial with a view to the adoption of ever more ecological practices. In particular, the estimation of emissions is necessary from the earliest stages of a project in order to enable timely solutions to minimise the generation of pollutants. With this in mind, the current work intends to provide a methodology capable of obtaining a preliminary estimate of emissions based on a few initial data, typical of the preliminary phase of a project. The proposed methodology is illustrated in figure 5.2 and is adapted to the SABRE in rocket mode, considered here as a case study. The objective of this work is to develop a propulsion system model for the SABRE engine in rocket mode, from which a propulsion database will be constructed. This step is preparatory to the creation of the emission database, which in this work will be calculated using the Cantera software. Since in the case study the combustion

	Parameters	Value	Reference
Preliminary	Altitude	25 - 90 [km]	[10]
	Propellant flow rate	796.97 [kg/s]	[10]
	Rocket operating time	282.9 [s]	[10]
	Mixture ratio	3 - 8	Assumed
	Hydrogen flow rate	88.55 - 199.24 [kg/s]	Assumed
	Oxygen flow rate	597.73 - 708.42 [kg/s]	Assumed
Liquid hydrogen tank	Tank pressure	2 [bar]	[10]
	Tank temperature	18 [K]	[10]
Liquid hydrogen pump	Efficiency	0.8	[9]
Hydrogen turbine	Efficiency	0.8	[20]
Liquid oxygen tank	Tank pressure	2 [bar]	[10]
	Tank temperature	80 [K]	[10]
Liquid oxygen pump	Efficiency	0.8	[9]
Liquid helium tank	Tank pressure	1 [bar]	[10]
	Tank temperature	4.2 [K]	[10]
	Helium mass flow rate	176.8 [kg/s]	[32]
Helium Turbine	Efficiency	0.8	[9]
	Turbine inlet temperature	1190 [K]	[32]
Helium compressor	Efficiency	0.8	[20]
	Compressor inlet temperature	51 [K]	[32]
	Compressor inlet pressure	53.8 [bar]	[32]
Combustion chamber	Combustion efficiency	0.9	[20]
	Pneumatic efficiency	0.95	[20]
	Lower calorific value	120.9 [MJ/kg]	[20]
	Combustion pressure	160 - 200 [bar]	Assumed
Nozzle	Pneumatic efficiency	0.98	[20]
	Efficiency	0.95	[20]
	Area Ratio	100	[32]
Heat exchanger	Pneumatic efficiency	0.9	[38]

Table 5.1: Input data for modelling the sabre in rocket mode

process does not produce NO_x, the Cantera software is used in this work to model the interaction between the rocket's exhaust gases and the atmosphere in which the aircraft is immersed, providing as input the data contained in the propulsive database. Using this tool, a systematic approach will be developed to generate a comprehensive emissions database, which in turn will be essential for developing

new methods for estimating emissions.

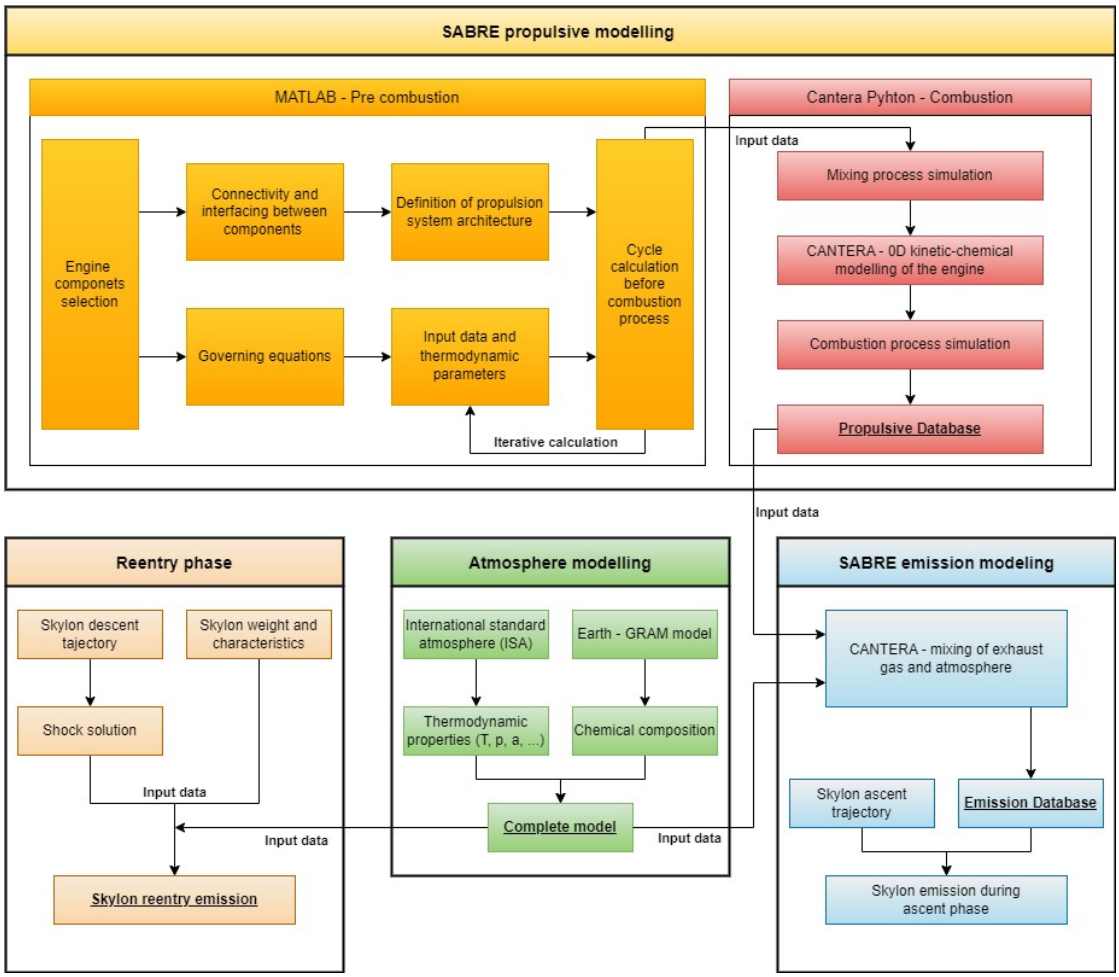

Figure 5.2: Skylon propulsive and emissive modelling workflow

5.2 Atmosphere modelling

Before proceeding with the description of the model of the SABRE in rocket mode, it is necessary to model the atmosphere with which the engine will interact. The need for modelling concerns in particular the composition of the atmosphere. The Skylon operates in rocket mode from an altitude of 25km, just above the troposphere, up to an altitude of 90km, which can already be considered the thermosphere: various layers of the earth's atmosphere are therefore crossed, which present different characteristics. In order to be able to appreciate these, it is therefore necessary to use an atmosphere model that takes them into account

and is able to replicate them. In the interest of this thesis, it is important to obtain a modelling of the atmospheric composition, because, especially at higher altitudes, there are significant variations in composition. This is not relevant in the troposphere, where the atmospheric composition is almost constant. In Matlab, there is a function that reports the International Standard Atmosphere (ISA), up to an altitude of 20km: in the latest versions released, it is possible to extend this function to also consider the stratosphere and mesosphere in the model. Unfortunately, this modelling only covers thermodynamic variables such as pressure, temperature, density, sound velocity and kinematic and dynamic viscosity, thus excluding the concept of composition. This limitation was overcome by using the Earth-Global Reference Atmospheric Model (GRAM) software developed by NASA [36]. This is a suite of atmospheric models that consider the average values of characteristic variables of the atmosphere and their statistical variations, obtained by interpolating data from direct measurements. It is possible to consider factors such as time variables, winds, geolocation and chemical composition in order to obtain specific results for a given trajectory. In this thesis work, only the average values given for the earth's atmosphere were used, because neither the trajectory that the Skylon will execute nor the spaceport from which it is intended to take off and land is known. The modelling of the Earth's atmosphere will be an input data for the realisation of the propulsive database, but above all of the emissive one: in fact, the composition of the atmosphere will be used to characterise the properties of the air flow in the atmosphere that will mix with the exhaust gases coming from the engine within the analysis carried out in Cantera. Figure 5.3 shows the profiles of the main variables describing the atmosphere.

5.3 SABRE pre-combustion modelling

The aim of this section is to explain the modelling of SABRE in the pre-combustion stages. The mathematical model developed in this thesis work involves the modeling of a rocket engine and as such is not directly influenced by altitude or flight speed except at the nozzle exit station. For these reasons, it is feasible to assume steady-state conditions for the SABRE in rocket mode at all internal stations. Similarly, a total-to-total approach is assumed for all internal engine stations for simplicity in mathematical analysis. However, the velocities involved in the internal stations are very low, therefore the two methods are practically coincident, but for accuracy, the approach described is preferred. The development of this part of the model was carried out entirely in Matlab, and part of the code can be seen in the appendix B. This is a choice dictated by the possibility of modelling hydrogen and oxygen using *Thermo* [19], a library on Matlab that is able to provide the thermodynamic characteristics of various gases over a very wide range of temperatures and pressures,

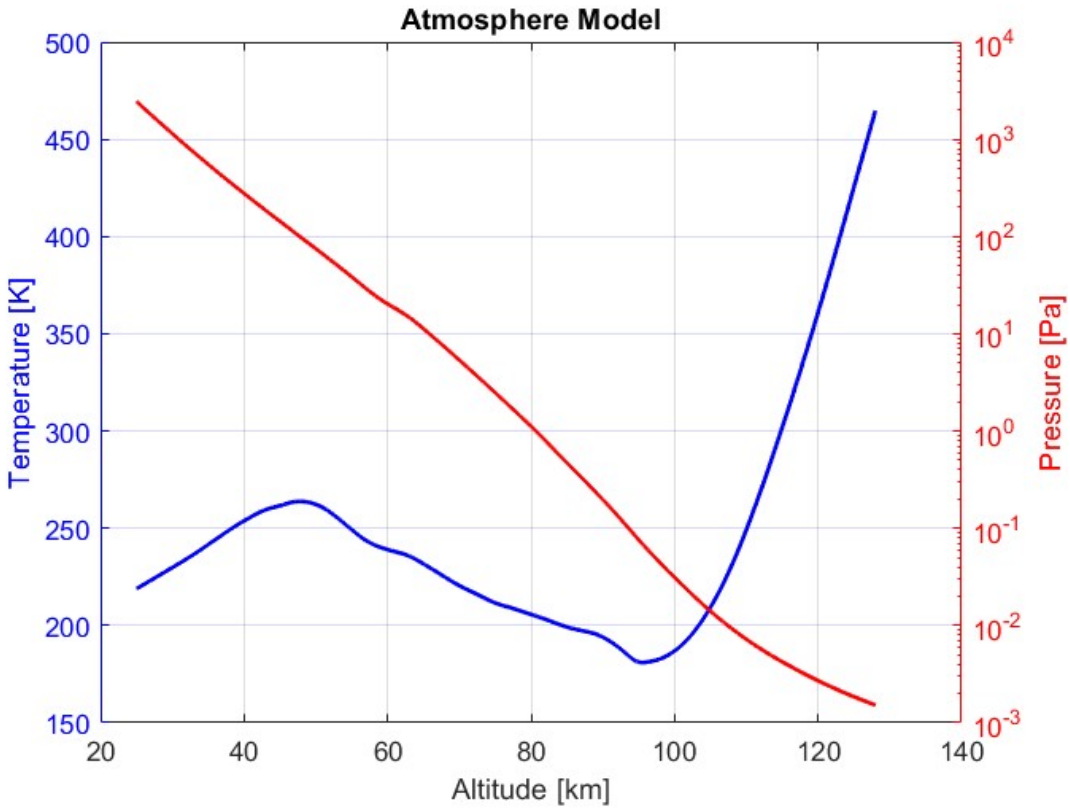

Figure 5.3: Atmosphere modelling

which includes all the combinations analysed within this part of the model, including cryogenic ones. Specifically, this library exploits the data in the National Institute of Standards and Technology (NIST) database, which is the most reliable in calculating these properties [21]. Once this object has been generated within the code and the operating pressure and temperature have been provided as input, this library is able to provide all the thermodynamic properties and in particular the specific heat at constant pressure and volume, c_p and c_v respectively. These are of primary importance in the further modelling for the calculation of all stations involved. The calculation of the physical quantities at a given station very often depends on the physical quantities themselves. It is therefore necessary to consider an iterative calculation across these stations to consider the update to convergence of these variables. This is the approach followed in the further analysis. An alternative to considering *themo-objects* for the calculation of thermodynamic properties could have been to use Cantera in its Matlab interface. However, it was preferred not to do this as Cantera does not include a pressure dependency in the calculation of specific heats and other properties. In fact, the modelling in

Cantera of these values is done by polynomial interpolation with 7 or 9 coefficients, all of which are dependent on temperature alone. This approach turns out to be too simplistic to be applied within this model as such pressures are reached that would generate too high an error: for instance, considering oxygen at standard temperature (300K) and at a standard pressure (1 [bar]) compared to considering the same gas at the same temperature but at an operating pressure of 200 [bar], generates a relative error of 23%. Furthermore, many of the kinetic schemes used to obtain the coefficients of polynomials describing the properties of a gas span very wide temperature ranges (e.g. 200K - 6000K) but do not include the cryogenic temperatures that are widely present within the SABRE. Due to the above, it is preferred to operate using *thermo-objects*. Unfortunately, helium has not yet been implemented within this library, so another solution had to be found to model the noble gas. In the first instance, it was thought to operate via Cantera's Matlab interface as the pressures involved here were considerably lower than in the other two circuits. However, this approach was avoided since, in the specific case of helium, the coefficients of the polynomial describing its thermodynamic properties turn out to be zero except for that relating to the known term. In this way, the dependence on temperature is also lost, in addition to the pressure as shown above. In consideration of all this, and recognising that there are only two helium-related stations that do not have the thermodynamic conditions assumed as known values, a manual iterative calculation using the NIST database was opted for. After obtaining convergence in the results, an analysis was carried out with respect to the previously proposed models. A maximum difference in the thermodynamic properties of 5% was revealed: in particular, considering only the temperature range for which the kinetic schemes are guaranteed, this difference to a value of less than 0.15%. Therefore, it can be stated that modelling using Cantera's Matlab interface is sufficiently accurate when applied to the modelling of non-cryogenic stations, while for cryogenic stations it is better to refer to the NIST database. The entire analysis was carried out considering different values of Mixture Ratio (MR), the ratio of mass flow rates of oxidant and propellant, so that this variable could be used as a free parameter. In particular, we opted to range between an MR of 3, a condition that maximizes the effective discharge velocity in a liquid Oxygen-Hydrogen combination, and 8, which represents the stoichiometric ratio between the two fuels considered and consequently coincides with the maximum achievable adiabatic flame temperature. In addition, modelling is carried out for two different combustion chamber pressure conditions of 160 and 200 [bar]. These pressures were taken into account as the air-breathing phase involves a combustion chamber at 160 [bar] while, in order to improve performance, it was preferred to carry out an analysis at a higher pressure, which is equal to the condition present in the Space Shuttle Main Engine (SSME). Finally, analyses were carried out both considering a zero heat exchange inside the liner, between combustion gases and

oxygen, and where this is equal to a fraction of the heat exchange that takes place inside the nozzle. The constraints to which the modeling is subject are physical and are related to two aspects: (i) cyclic conditions of the helium circuit and (ii) shaft work in the helium compressor assembly and second hydrogen turbine. Specifically, the cyclic conditions in the helium circuit require that at the end of the calculation in the helium cycle modeling, the same conditions that were imposed as input in station [11], downstream of HX3, are obtained. Second, it is verified that the energy extracted in the expansion of the second hydrogen turbine is the same as the energy required to move the helium circulator. As long as these conditions are not verified, the code continues to iterate by changing the compression coefficient of the hydrogen turbopump, which during the first iteration is set to a hypothetical value. In the following, the hydrogen, oxygen and helium circuits are analysed and the individual stations shown in the diagram in the figure 5.1 are explained.

5.3.1 Hydrogen Circuit

- 0: As reported by REL [10], liquid hydrogen is stored in cryogenic tanks at a temperature of 16 K and a pressure of 2 [bar];
- 0-1: Through a turbo-pump, hydrogen is compressed to suitable pressures for achieving a combustion chamber pressure of 160 or 200 [bar];

$$P_{LHP} = \dot{m}_{H_2} \cdot \frac{p^{\circ}_{H_2,1} - p^{\circ}_{H_2,0}}{\eta_c \cdot \rho_{H_2,0}}$$

$$T^{\circ}_{H_2,1} = T^{\circ}_{H_2,0} + (\frac{1-\eta_c}{\eta_c} \cdot (\frac{P_{LHP}}{\dot{m}_{H_2} \cdot c_{p,H_2}})$$

- 1-2: Inside the HX 4, helium transfers energy to hydrogen;

$$p^{\circ}_{H_2,2 = p^{\circ}_{H_2,1} \cdot \epsilon_{HX}}$$

$$T^{\circ}_{H_2,2} = T^{\circ}_{H_2,1} + \frac{P_{HX4}}{\dot{m}_{H_2} \cdot c_{p,H_2}}$$

- 2-3: Hydrogen, now in gaseous form after passing through the HX, expands in a turbine and drives its own turbo-pump;

$$W_{t,2-3} = \frac{P_{LHP}}{\dot{m}_{H_2}}$$

$$T^{\circ}_{H_2,3} = T^{\circ}_{H_2,2} - \frac{W_{t,2-3}}{c_{p,H_2}}$$

$$p^{\circ}_{H_2,3} = \frac{p^{\circ}_{H_2,2}}{\beta_{t,2-3}}$$

- 3-4: Hydrogen undergoes a second expansion in a turbine and drives the compressor and the entire helium circuit. The temperature downstream of this second expansion is sufficiently high, eliminating the need to use the propellant as a coolant for the Combustion Chamber (CC);

$$T^{\circ}_{H_2,4} = T^{\circ}_{H_2,3} - \frac{P_{t,3-4}}{\dot{H}_2 \cdot c_{p,H_2}}$$

- 4-8: Hydrogen is mixed with oxygen and is now ready to react in the main CC.

The values of the reference thermodynamic quantities at the various stations of the hydrogen circuit are shown in the figure 5.4.

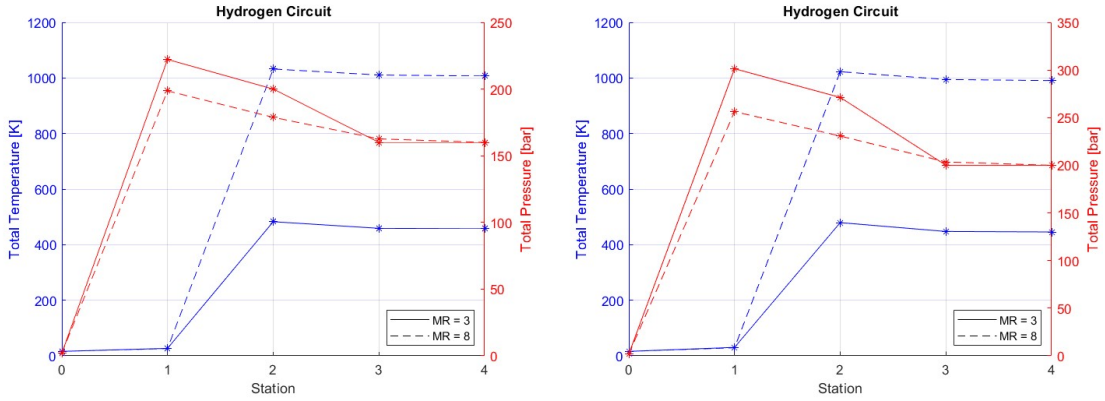

Figure 5.4: thermodynamic quantities at hydrogen circuit stations in case of 160 and 200 [bar] CC pressure, respectively

5.3.2 Oxygen Circuit

- 5: As reported by REL [10], liquid oxygen is stored in cryogenic tanks at a temperature of 80 K and a pressure of 2 [bar];

- 5-6: Through a turbo-pump, oxygen is compressed to suitable pressures for achieving a combustion chamber pressure of 160 or 200 [bar];

$$\beta_{O_2,5-6} = \frac{p_c/\epsilon_{HX}}{p^{\circ}_{O_2,5}}$$

$$p^{\circ}_{O_2,6} = \beta_{O_2,5-6} \cdot p^{\circ}_{O_2,5}$$

$$P_{LOP} = \dot{m}_{O_2} \frac{p^\circ_{O_2,6} - p^\circ_{O_2,5}}{\eta_c \cdot \rho_{O_2,5}}$$

$$T^\circ_{O_2,6} = T^\circ_{O_2,5} + \frac{1-\eta_c}{\eta_c} \cdot \frac{P_{LOP}}{\dot{m}_{O_2} \cdot c_{p,O_2}}$$

- 6-7: Oxygen, still at cryogenic temperatures, is used as a coolant for the combustion chamber to prevent damage to the liner and other elements. Additionally, this process regenerates the oxygen, which, upon entering the combustion chamber at higher temperatures, ensures higher performance;

$$p^\circ_{O_2,7} = p^\circ_{O_2,6} \cdot \epsilon_{HX}$$

$$T^\circ_{O_2,7} = T^\circ_{O_2,6} + \frac{P_{HX,liner}}{\dot{m}_{O_2} \cdot c_{p,O_2}}$$

- 7-8: Oxygen is mixed with hydrogen and is now ready to react in the main CC.

The values of the reference thermodynamic quantities at the various stations of the Oxygen circuit are shown in the figure 5.5.

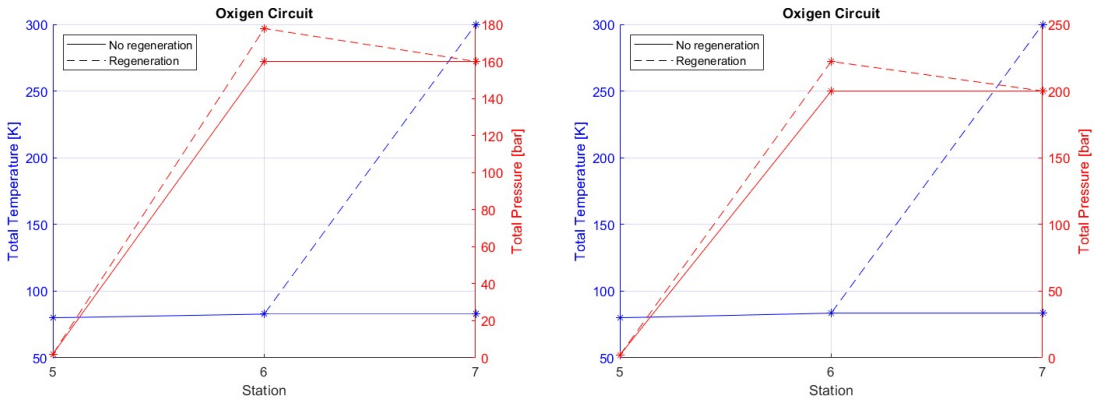

Figure 5.5: thermodynamic quantities at Oxygen circuit stations in case of 160 and 200 [bar] CC pressure, respectively

Unlike the hydrogen cycle, where the turbo-pump compression ratio cannot be predefined due to its interdependence with the rest of the model, for the oxygen cycle it is possible to directly calculate the compression ratio of the turbo-pump.

5.3.3 Helium Cycle

- 11-12: Helium flow is processed by a compressor, driven by the second turbine of the hydrogen circuit, which increases its pressure and provides the necessary energy for continuous movement within the circuit. For this reason, this component is referred to as a circulator;

$$T^{\circ}_{He,12} = T^{\circ}_{He,11} \cdot \left(1 + \frac{1}{\eta_c} \cdot \left(\beta_{c,11-12}^{\frac{\gamma_{He}-1}{\gamma_{He}}} - 1\right)\right)$$

- 12-13: Helium reaches the nozzle where it acts as a heat sink for the hot flows generated in the main CC, heating the nozzle walls as it flows through. During this phase, helium absorbs energy which it will later transfer to other stations along the cycle.

$$P_{HX,nozzle} = \dot{m}_{He} \cdot c_{p,He}(T^{\circ}_{He,13} - T^{\circ}_{He,12})$$

- 13-14: Gaseous helium expands in the turbine connected to the turbo-pump of the oxygen circuit to ensure its proper operation;

$$p^{\circ}_{He,13} = p^{\circ}_{He,14} \cdot \beta_{t,13-14}$$

$$T^{\circ}_{He,14} = T^{\circ}_{He,13} - \frac{W_{t,13-14}}{c_{p,He}}$$

- 14-11: The HX4, named to maintain consistency with the previous modeling, allows helium to transfer heat and energize the hydrogen circuit. Since the helium cycle is closed, it is essential that the initial and final conditions correspond to ensure proper operation in subsequent cycle simulations.

$$p^{\circ}_{He,14} = \frac{p^{\circ}_{He,11}}{\epsilon_{HX}} \epsilon_{HX}$$

$$P_{HX4} = \dot{m}_{He} \cdot c_{p,He}(T^{\circ}_{He,14} - T^{\circ}_{He,11})$$

The values of the reference thermodynamic quantities at the various stations of the Oxygen circuit are shown in the figure 5.4.

The helium cycle is a regenerative cycle that facilitates the transfer of significant amounts of energy between different zones of the propulsion system. It is the circuit that differs most from the modeling of the air-breathing phase. Specifically, helium is energized only at the nozzle, contrasting with the earlier modeling approach. Cooling the nozzle walls during the rocket phase is crucial for reusable spacecraft like Skylon. Without a cooling solution, the walls would not withstand prolonged and repeated use. Helium, unlike other propellants onboard, is chosen because this is the only source of heat available during the rocket phase for energizing the system.

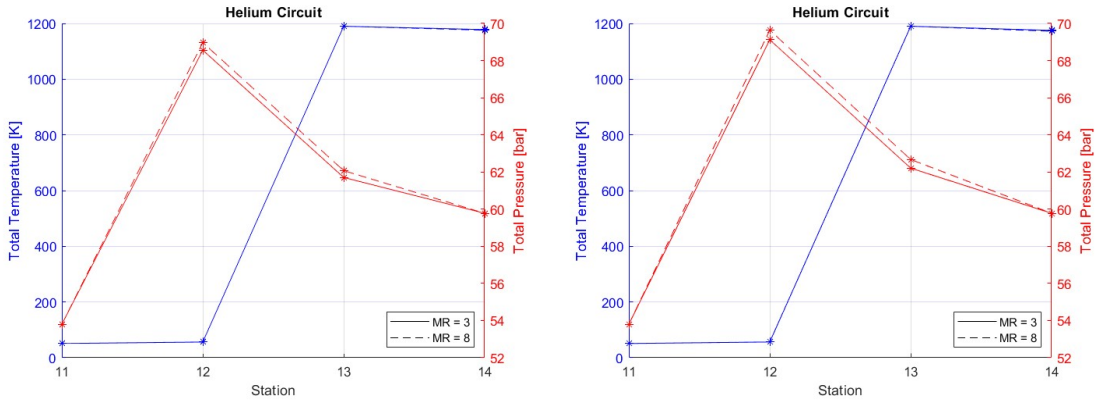

Figure 5.6: thermodynamic quantities at Helium circuit stations in case of 160 and 200 [bar] CC pressure, respectively

5.4 SABRE combustion and post-combustion modelling

The aim of this section is to expose the modelling of the combustion and exhaust gas circuit in rocket mode. This was realised using Cantera in its Python interface, as this interface has more libraries and functions than the Matlab interface. In particular, the results from the Matlab modelling of the pre-combustion stations are taken as input for the combustion model in Python, and in particular the characteristics of the two flows, in terms of flow rates, temperatures and pressures, are considered: with these simple parameters, combustion can be simulated. Despite the fact that the interaction of LOX and LH2 only generates water vapour and at most unburnt or atomic elements, combustion is realised by considering the kinetic scheme $z24\_nox$, which also considers reactions for the generation of nitrogen oxides. This is done in order to obtain continuity in the results generated: in fact, the same scheme is then used to consider the mixing of the exhaust gases with the surrounding atmosphere. Before proceeding with the simulation of the combustion process, it is necessary to consider the mixing of the two flows. This is possible in Cantera by making a simple sum of the two flows considered, but before adding them up, it is necessary to characterise them with their properties. In particular, it is imposed pressure, temperature, composition and finally the quantity considered, as can be seen in the figure 5.7.

Combustion is a process that is simulated in Cantera as a succession of consecutive non-equilibrium states. Indeed, it is thanks to this condition that compounds are obtained that in software such as Chemical Equilibrium with Application (CEA)

```
gasO2 = ct.Solution('YAML\z24.yaml')
gasH2 = ct.Solution('YAML\z24.yaml')
# Stream O2, si utilizza constant='HP' perchè ho la pressione costante nel mixing
gasO2 = ct.Quantity(gasO2, constant='HP')
# y sono frazioni in massa, x sono frazioni molari
gasO2.TPY = Tox[a], P_mix, 'O2:1'

# Stream H2
gasH2 = ct.Quantity(gasH2, constant='HP')
gasH2.TPY = Tf[a], P_mix, 'H2:1'

# Set the molar flow rates
gasO2.moles = Mox[a]
gasH2.moles = Mf[a]

# Compute the mixed state
M = gasO2 + gasH2
```

Figure 5.7: Pre-combustion mixing in Cantera

are not possible. In particular, a network of batch reactors is generated within the code, which is made to evolve over time by means of the *step()* command. In this analysis, it was necessary to consider an igniter because the temperatures of the mixed flows are lower than the self-ignition temperature of hydrogen, which is listed in the table 4.1. This element provides the energy needed to ignite combustion. From the results of this time analysis, it is possible to extract various information that is useful for characterising combustion. In particular, it is possible to obtain:

- the Ignition Delay Time (IDT), is the time interval between the start of the simulation and the ignition of the mixture inside the chamber. There are various methods to determine this, but the most accurate is the method of observing the first peak in the mass fraction of hydroxyl radicals. At this peak, the reaction can be considered to have started;
- the mass fractions of all species considered in the kinetic scheme at the start of combustion;
- the Adiabatic Flame Temperature (AFT) obtained under equilibrium conditions, i.e., for much longer times than IDT.

Having reached this stage of the combustion analysis, it was decided to carry out a dual analysis as a function of the IDT and the residence time inside the combustion chamber. In particular, considering the case study in which oxygen is regenerated by the heat extracted from the liner, two possible solutions can be

derived. The first involves considering, as done in the non-regenerated case, the condition of leaving the chamber at a time equal to IDT. However, it is possible to consider as an exit condition the one for which the time instant coincides with the IDT of the non-regenerated condition. In this case, it is as if one were studying the flow in the regenerated condition with the same residence time with respect to the non-regenerated condition. In figure 5.8, it is possible to observe the IDT in the regenerated and non-regenerated conditions as a function of the MR.

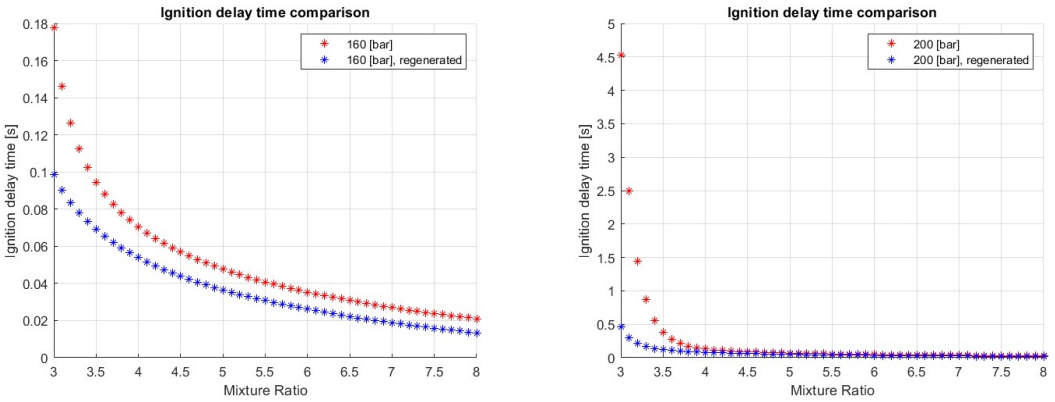

Figure 5.8: IDT in combustion at 160 and 200 [bar], respectively

It should be noted that the times obtained are always shorter for regenerated cases than for non-regenerated ones. This can be attributed to a physical aspect of combustion: in fact, by providing higher inlet temperatures, it is taken for granted that ignition of the mixture will take less time. Having lower IDT allows the size, and thus the volume, of the combustion chamber to be limited. What is most interesting is certainly the comparison of ignition times as the pressure in the chamber varies under the same regeneration conditions, which can be seen in the figure 5.9.

It can be seen that for higher pressures the IDT are greater: the reasons for these trends lie in the reactive pathways associated with hydrogen combustion. Although at an early stage in the hydrogen explosivity diagram, an increase in pressure favours combustion, this is not valid in absolute terms. In particular, in the case of very high pressures, as in the case of studies, intermediate compounds such as H2O2 are generated, which slow down the combustion process. Conversely, for lower pressures, hydroxyl radicals are formed, which are much faster and speed up combustion [27]. The analysis proceeds by taking an overview of the end combustion temperatures obtained in the different cases under analysis. In the figure 5.10, it is possible to note the trends as the MR varies, and it can be seen that the regenerated case, which has residence times equal to those of the

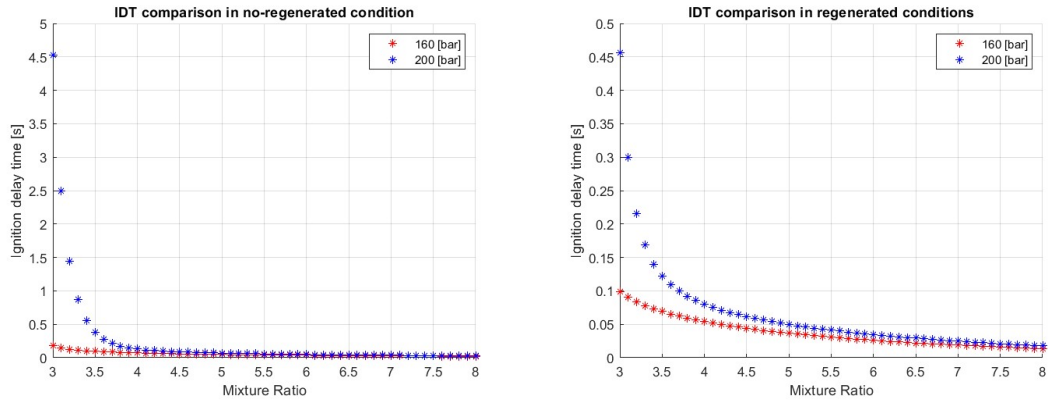

Figure 5.9: IDT in combustion under non-regenerated and regenerated conditions, respectively

non-regenerated case, develops the highest temperatures. This is obvious as the mixture, reaching ignition earlier, has more time to proceed with combustion and approach an equilibrium condition and the AFT.

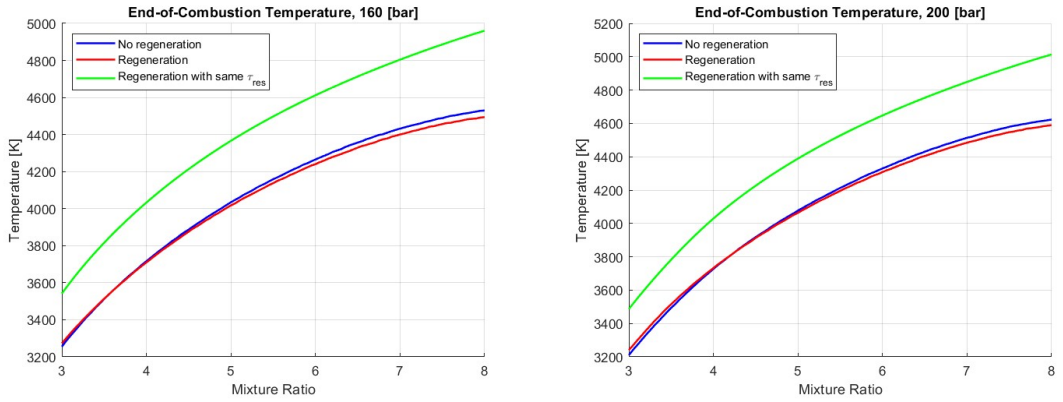

Figure 5.10: End combustion temperature at 160 and 200 [bar], respectively

Once the combustion process is complete, it is intended, as was done previously, to analyse the exhaust gas circuit and characterise the individual stations. To analyse the thermodynamic properties of the flue gas mixture, Cantera was used in its Python interface, as it is able to consider all chemical species within it.

5.4.1 Exhaust Gas Circuit

- 8: This station is downstream of combustion where the two mixed flows have reacted and completed combustion;
- 8-9: At this station, heat exchange at the nozzle wall between the hot exhaust gas flow and the helium cycle is simulated. It has been modeled as a HX that generates pressure losses only on the noble gas side. This is because only helium is forced to pass through the small holes in the nozzle walls, allowing the hot exhaust gas flow to expand freely in the nozzle without experiencing pressure losses;

$$T^{\circ}_{Ex,9} = T^{\circ}_{Ex,8} - \frac{P_{HX,liner}}{\dot{m}_{EX} \cdot c_{p,Ex}}$$

- 9-10: This is the nozzle of the propulsion system. It is modeled as a single nozzle for all 8 combustion chambers present in the two SABRE engines mounted at the ends of the wings. In this section, a total-to-static approach is used, unlike all the other stations that prefer a total-to-total approach since they are internal;

$$w_{10} = \sqrt{\frac{2\gamma_{Ex}}{\gamma_{Ex} - 1} R T_c \left[1 - \left(\frac{p_e}{p_c}\right)^{\frac{\gamma_{Ex-1}}{\gamma_{Ex}}}\right]}$$

$$T_{Ex,10} = T^{\circ}_{Ex,9} - \frac{w_{10}^2}{2c_{p,Ex}}$$

- 10: This is the interface station between the hot flow from the engine and the surrounding environment, which becomes increasingly rarefied as ascent progresses. At this station, analysis is conducted on the interaction between the combustion exhaust gases and the surrounding atmosphere to study the resulting products.

The values of the thermodynamic reference quantities at the various stations of the exhaust gas circuit are shown in the figures 5.11, 5.12 and 5.13.

5.5 Propulsive database

In this section of the thesis work, it is intended to present the performance of the SABRE derived from the propulsion model. Since it is a launcher, the first parameter to be analysed in order to understand the performance is the calculation of the velocity change that the SABRE is able to provide during its ascent in rocket

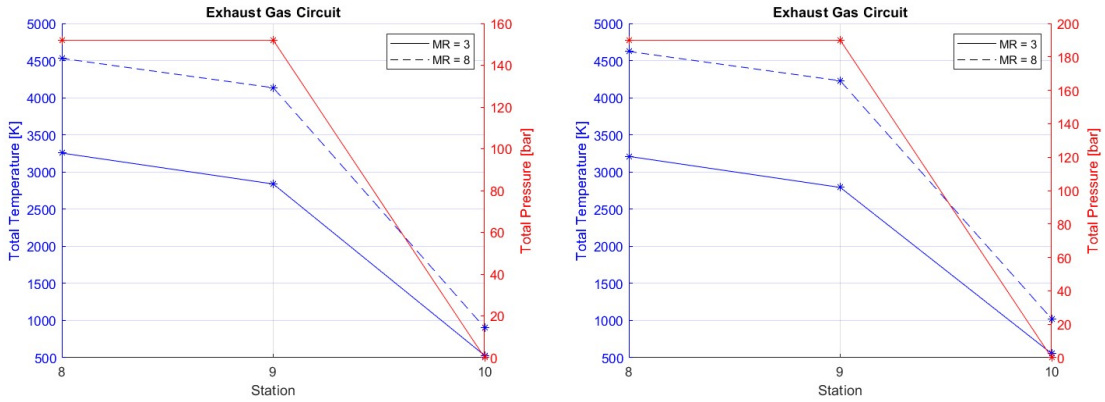

Figure 5.11: Thermodynamic quantities at exhaust gas circuit stations in the non-regenerated case at 160 and 200 bar, respectively

mode. This parameter can be calculated using the Tsiolkovsky rocket equation, given hereafter:

$$\Delta V = I_{sp}\, g_0 \cdot \ln\left(\frac{M_i}{M_f}\right) \tag{5.1}$$

where I_{sp} is the specific impulse, M_i the initial mass and M_f the final mass of the launcher. After calculating the specific impulse, involved in the equation, by using the ideal rocket model, the values associated with the various configurations are derived and listed in the table 5.2.

	Non-regenerated case		**Regenerated case**		**Regenetare with same τ_{res}**	
P**Pressure**	**MR = 3**	**MR = 8**	**MR = 3**	**MR = 8**	**MR = 3**	**MR = 8**
160 [bar]	4.598 [km/s]	5.003 [km/s]	4.956 [km/s]	5.001 [km/s]	5.002 [km/s]	5.039 [km/s]
200 [bar]	6.241 [km/s]	6.301 [km/s]	6.204 [km/s]	6.264 [km/s]	6.256 [km/s]	6.306 [km/s]

Table 5.2: ΔV comparison obtained in the analysed configurations

It can be seen immediately that the case analysed at lower pressure (160 [bar]), in all the configurations considered, does not meet a minimum velocity variation requirement that would guarantee reaching low earth orbit. On the other hand, the 200 [bar] configuration does provide this variation. In fact, if it is considered to

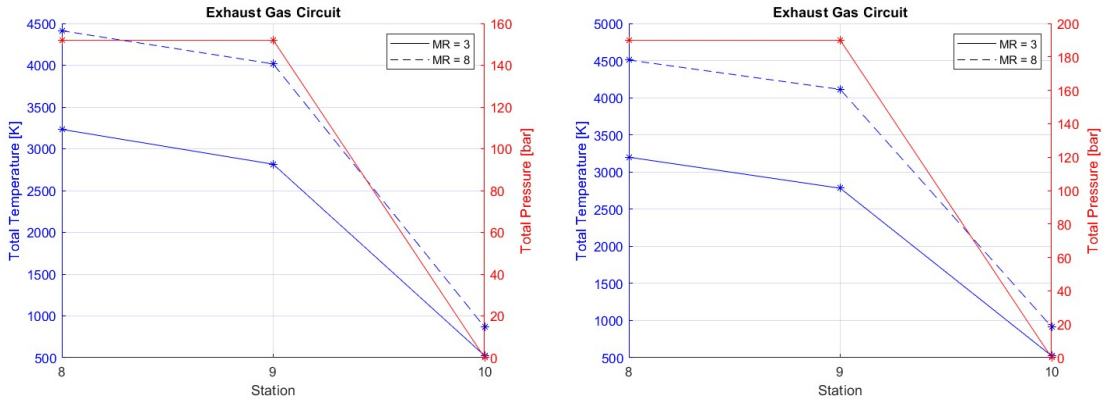

Figure 5.12: Thermodynamic quantities at exhaust gas circuit stations in the regenerated case at 160 and 200 bar, respectively

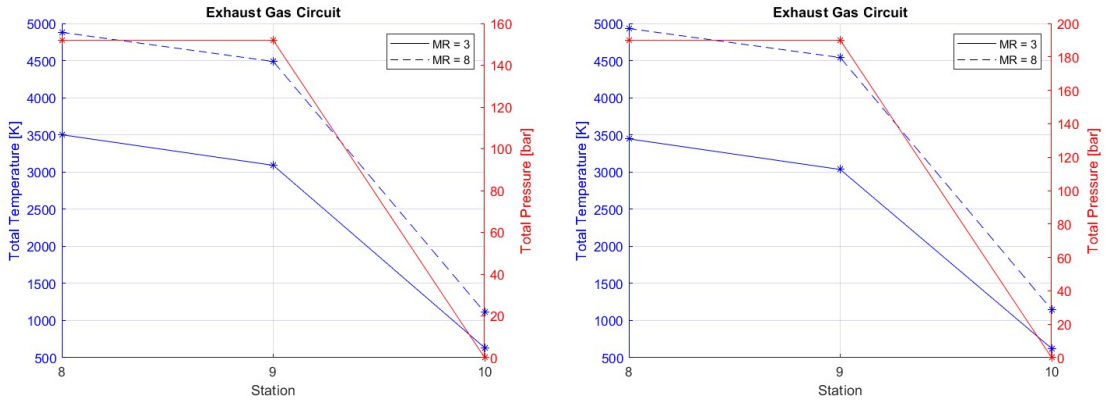

Figure 5.13: Thermodynamic quantities at exhaust gas circuit stations in the regenerated case considering the same τ_{res} at 160 and 200 bar, respectively

start from a velocity of about 1.5 [km/s] at the beginning of the rocket phase [10], this variation allows a final velocity, in the worst case analysed, of 7.7 [km/s], which is a sufficient value to reach the desired orbit. In fact, it must not be forgotten that it is the Skylon Orbital Manoeuvring Assembly (SOMA) that provides the last impulse for the circularisation of the orbit once the predetermined altitude has been reached. Therefore, the continuation of the discussion will only consider this configuration. The other characteristic features of a launcher are now analysed and compared with what is expressed by REL.

In particular, in figure 5.14, it is possible to observe the specific impulse as a function of altitude and parameterised as a function of MR and regeneration. It can

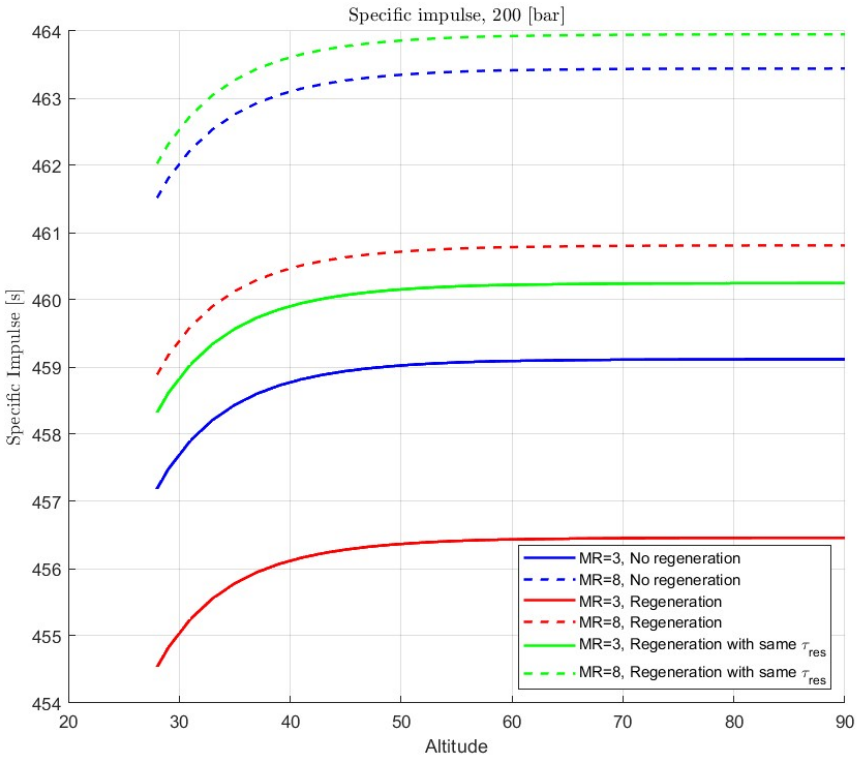

Figure 5.14: Specific impulse at 200 [bar] considering all conditions

be observed how the values obtained are very similar to the 450 [s] reported by REL and, moreover, as the best combinations involve MR equal to the stoichiometric one. In fact, in this condition, the highest AFT is obtained, which allows for superior performance. It should also be noted that the condition with a lower chamber volume is the one with the worst performance. This can be attributed to the fact that the end combustion temperature is very similar to that obtained in the non-regenerated case, as shown in figure 5.10, but, due to the heat subtraction that takes place in the liner, it has worse characteristics than the other configurations in the other stations of the circuit, as can be seen in the figures 5.11, 5.12 and 5.13.

Figure 5.15 shows the thrust trend that the SABRE provides to the Skylon during ascent into orbit as a function of altitude. these values were obtained by considering the following equation:

$$T = c \cdot \dot{m}_{tot}$$

These values are slightly lower than those indicated by REL within [10], although within the manual reference is made to the gross thrust while the calculated one

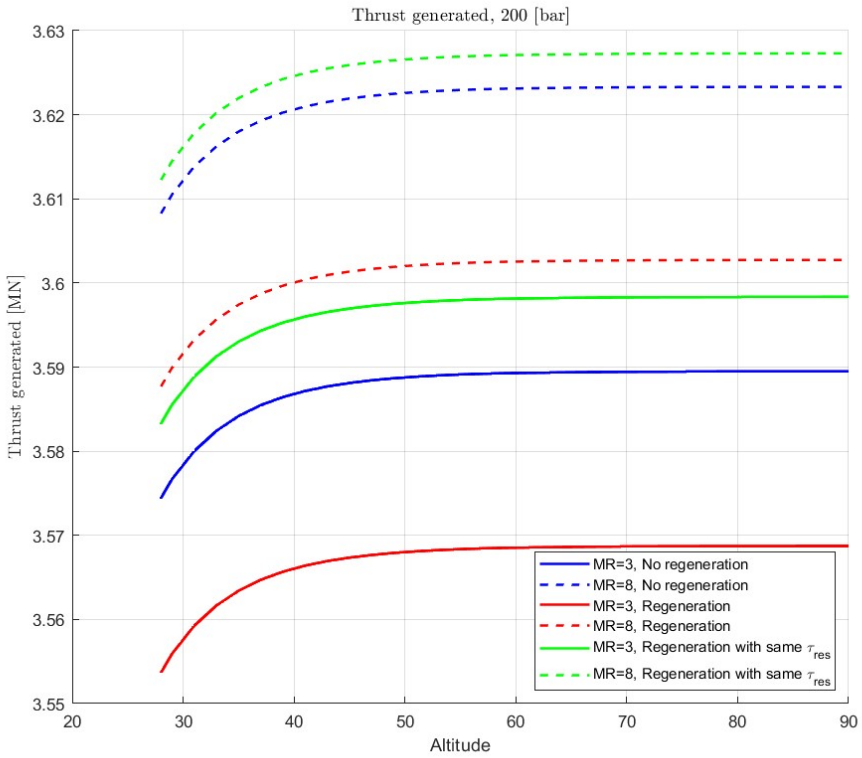

Figure 5.15: Thrust generated at 200 [bar] considering all conditions, according to the formula $[T = c \cdot \dot{m}_{tot}]$

already considers any losses due to the additional resistance generated when the engine is placed on-board and in the atmosphere. However, it is possible to calculate the thrust generated by considering the classical thrust formulation below:

$$T = \dot{m}_{tot} \cdot w_{10} + A_e \cdot (p_e - p_0)$$

where p_e is the static pressure at the nozzle outlet and p_0 is the ambient pressure. Figure 5.16 shows the thrust trend obtained with this second formulation. It can be seen that these values are similar in the case of stoichiometric combustion, while they are considerably lower in the case of fuel-rich combustion. It can also be seen that the variation along the altitude is more limited than that calculated previously.

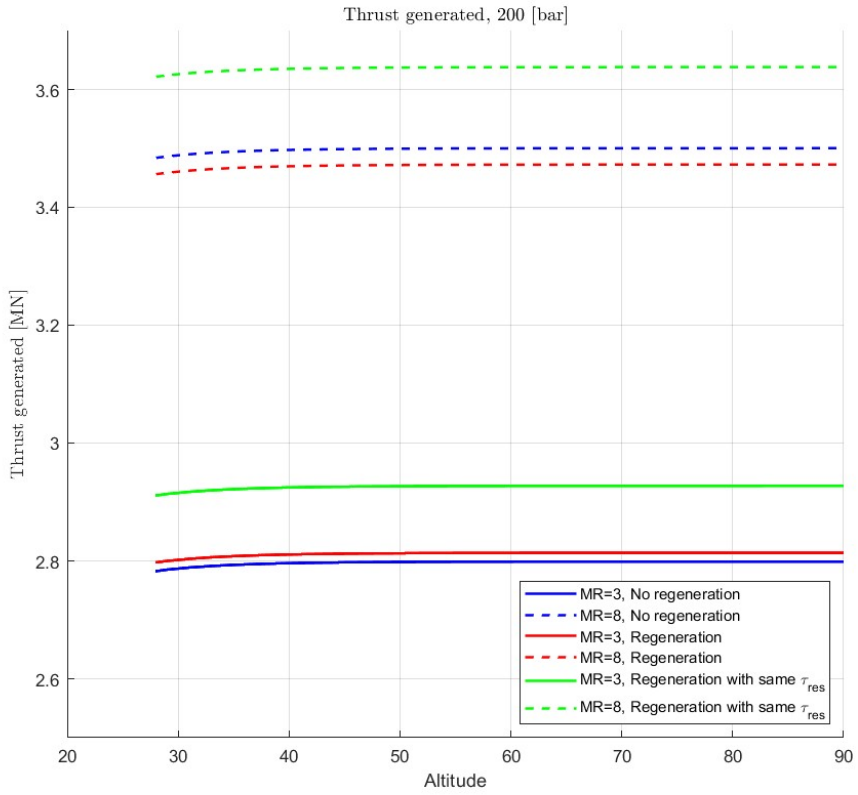

Figure 5.16: Thrust generated at 200 [bar] considering all conditions, according to the formula $[T = \dot{m}_{tot} \cdot w_{10} + A_e \cdot (p_e - p_0)]$

5.6 Emissive database

The purpose of this section is to recall the method by which the emission database was realised and to analyse the results obtained. The emissive database has been realised starting from a few inputs, such as, the atmosphere model and the propulsive database presented above: in particular, each engine station is composed of thermodynamic data, such as pressure and temperature, but also of chemical data and, specifically, the mass compositions at each engine station are known, including station [10], i.e. the interface between the engine output and the external atmosphere. The variables just listed are sufficient to carry out the emission analysis of the SABRE in rocket mode. As in the case of combustion, the use of Cantera, in its Python interface, is used to study and analyse the mixing and interaction of the exhaust gas flow from the engine with the surrounding atmosphere. Before proceeding, it is intended to specify that the composition of the exhaust gas at

the nozzle is assumed to be equal to that at the combustor outlet. This is a typical assumption for rocket propulsion systems since, once combustion has taken place, the residence time inside the engine is very limited and due to the strong expansion and cooling that occurs at the nozzle it is plausible to consider the flow as 'frozen'. The kinetic scheme considered for the analysis is, as with combustion, the $z24\_nox$, which allows the formation of nitrogen oxides to be analysed. In this case, it is not necessary to perform a time-dependent analysis as it is the final equilibrium state that is of interest in order to obtain the emissions generated by the engine. Therefore, it is sufficient to carry out the mixing of the two flows, wait for their reaction and observe the compounds generated in the equilibrium state. In particular, the *EQUILIBRATE('HP')* command is used to carry out an analysis under conditions of constant pressure and enthalpy. In order to carry out the mixing, it is necessary to characterise the two flows considered: the flow of hot gases from the engine will be characterised according to the propulsive database obtained previously, in terms of temperature, pressure and flow rate as well as chemical composition. With regard to the surrounding atmosphere, on the other hand, the discourse is slightly different: the modelling of the atmosphere, reported in 5.2, provides the values of temperature, pressure and chemical composition but the flow rate is not defined. After careful analysis and several empirical tests, it was decided to allow for an air flow rate of fifty times that expelled by the engine. The reasoning behind this decision is related to the fact that unburnt hydrogen, if present, needs a sufficient amount of air in order to react, so a sufficient air flow rate must be considered. Following several tests, it was noted that, due to the fact that enthalpy is considered constant in the equilibrium analysis, considering air flow rates of the order of magnitude of those emitted by the engine does not allow a stable equilibrium to be achieved. Consequently, it was decided to consider an air flow rate significantly higher than that expelled by the engine, i.e. in a ratio of 50:1. Before proceeding with the calculation of $EINO_x$, it is necessary to explain the formulation with which these indices have been calculated. Usually, $EINOs$ are calculated using the following formula:

$$EINO_x = 10^3 \cdot \frac{Y_{NO_x}}{Y_{H_2,in} - Y_{H_2,out}} \; [g/kg]$$

i.e., considering only the mass fractions of the analysed species. This is possible as all terms refer to the same amount of matter that is processed by the engine at a precise instant. However, using the approach just presented, this formulation is no longer valid as the individual terms refer to different quantities of matter. For this reason, we work by considering flow rates instead of mass fractions, resulting in the following relationship:

$$EINO_x = 10^3 \cdot \frac{\dot{m}_{NO_x}}{\dot{m}_{H_2,in} - \dot{m}_{H_2,out}} \; [g/kg]$$

Figure 5.17 shows the trends of $EINO_x$ calculated as flight altitude varies and parameterised as a function of oxygen regeneration condition.

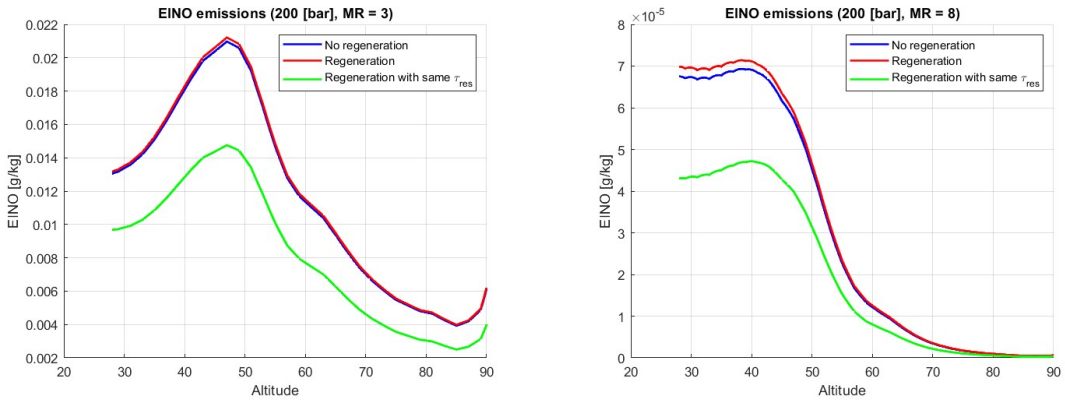

Figure 5.17: $EINO_x$ production trend as a function of altitude under conditions of MR of 3 and 8, respectively

It can be seen that the regenerated case, which considers the same combustion chamber volume as the non-regenerated case, performs best in terms of environmental impact. In fact, a longer residence time in the combustion chamber allows a higher combustion feed rate to be considered, which reduces the unburned hydrogen present in the flow. A further aspect that must be considered is related to the emissions generated in the stoichiometric MR configuration: the amount of $EINO_x$ produced in this configuration is several orders of magnitude lower than those obtained in the case of fuel-rich combustion. The explanation behind this phenomenon is linked to the post-combustion that takes place in the atmosphere in the presence of unburnt hydrogen: the high temperatures of the exhaust gases guarantee this reaction, which releases further energy by reaching temperatures sufficient for the formation of nitrogen oxides. For this reason, in terms of emission performance for NO_x, the best solution is the one with MR close to the stoichiometric one. It should be noted that many of the aspects analysed above, in the context of limiting nitrogen oxide emissions, run counter to the solutions adopted by air-breathing engines. Indeed, in that case, lower combustion temperatures, fuel-rich mixture ratios and limited residence times are preferred in order to avoid the formation of nitrogen oxides. In the following analysis, it is intended to apply these indices to an ascent trajectory and derive the Skylon's total emissions during

a launch. As the Skylon's trajectory is not available, it is derived from the data provided by REL, in the figure 3.2. From these graphs, by sampling the data, it is possible to derive a series of functions of quantities such as altitude, velocity, mach and mass as a function of time. These provide a first approximate trajectory which is used in the further analysis. Once it is known the emission rates at each altitude, the trajectory and the time the aircraft flies at a certain altitude, it is possible to derive the total emissions of nitrogen oxides expressed as a function of the height at which they are emitted. In particular, it is sufficient to perform a multiplication between the emission indices, the total flow rate considered and the time for which the aircraft flies at a certain altitude. The results are shown in the figure 5.18.

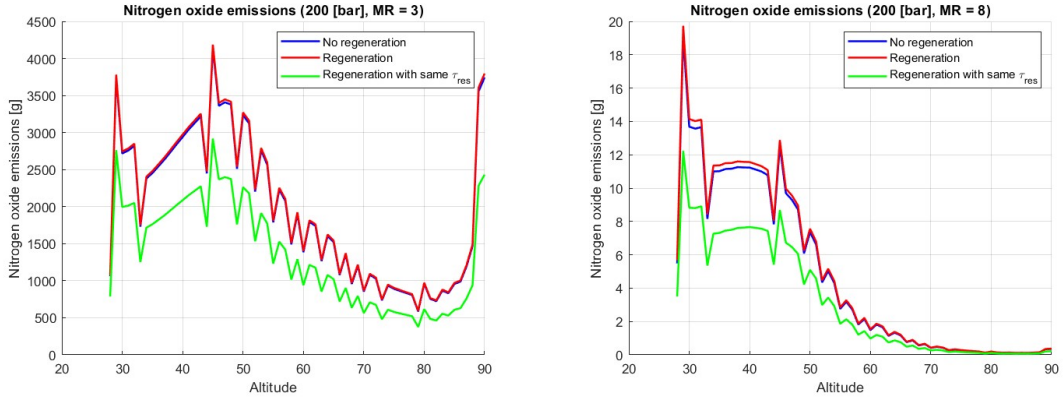

Figure 5.18: Emissions of NO_x generated during the ascent trajectory as a function of altitude at MR 3 and 8, respectively

The very irregular pattern in the graphs is due to the lack of accuracy in the flight trajectory and especially in the definition of the time intervals at which the aircraft is at a specific altitude. As reported in the section 2.2, it is not only nitrogen oxides that have an environmental impact, but also water vapour dispersed into the atmosphere, especially at high altitudes, is impactful. For this reason, the figure 5.19 shows the water vapor emissions as a function of altitude. It can be seen that the emissions generated by the fuel rich condition are significantly higher than those generated under stoichiometric conditions. Again, the reason for this is associated with the amount of unburned hydrogen which, once dispersed in the atmosphere, can react with an additional mass of oxygen and generate further water vapour.

Finally, it is reported the total emissions of the two pollutants considered in this analysis throughout the rocket ascent phase: these values can be seen in the table 5.3.

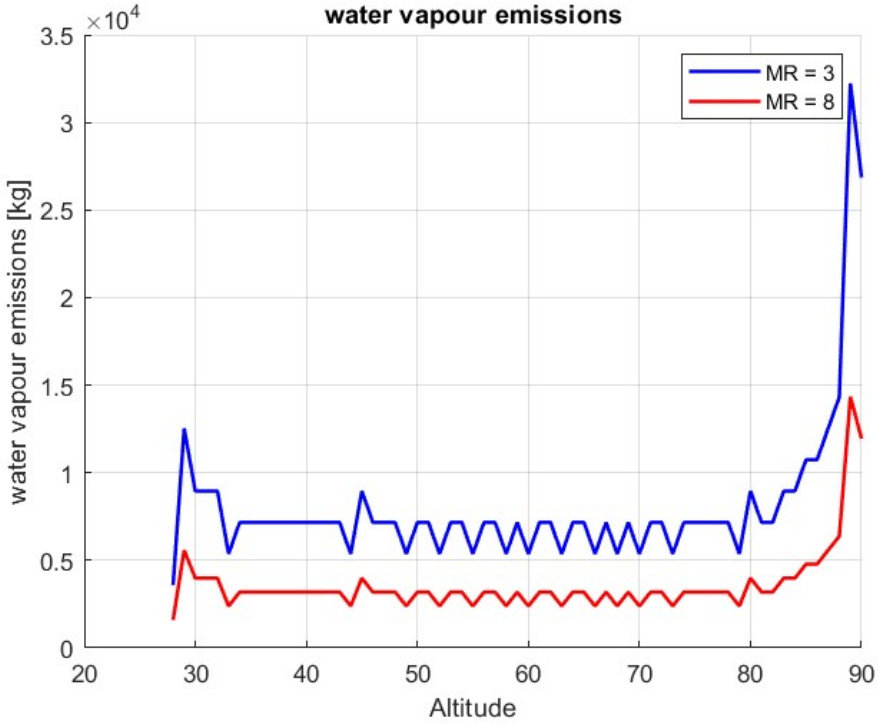

Figure 5.19: Emissions of NO_x generated during the ascent trajectory as a function of altitude at MR 3 and 8, respectively

	Non-regenerated case		**Regenerated case**		**Regenetare with same τ_{res}**	
Species	**MR = 3**	**MR = 8**	**MR = 3**	**MR = 8**	**MR = 3**	**MR = 8**
NO_x [kg]	123.886	0.295	125.376	0.304	85.662	0.198
H_2O [kg]	506724	225462	506724	225463	506724	225463

Table 5.3: Total emissions released into the atmosphere during the ascent phase

Chapter 6

Skylon reentry phase

In this chapter of the thesis, the focus is on analyzing the re-entry phase of the Skylon spaceplane. This phase is one of the most critical parts of the mission due to the extremely high temperatures that occur as the vehicle interacts with the surrounding atmosphere. During re-entry, thermal and structural resistance is ensured by the materials used both internally and on the outer surface exposed to the high-temperature flow, specifically the lower fuselage and wings. The primary structure consists of a frame made from titanium elements reinforced with silicon carbides. This frame is subsequently covered with sheets of glass-ceramic materials that serve both as an aeroshell and as the first line of thermal protection, which is further enhanced by a multi-layered metallic heat shield. The management of thermal flows, in addition to the materials used, is heavily dependent on the aerodynamics of the vehicle. It is crucial for the vehicle to maintain a well-defined attitude capable of handling the heat and stresses generated during this phase. The re-entry must begin at a precise pre-calculated moment to ensure landing at the designated spaceport. Specifically, at an altitude of 120 km, the Skylon initiates a retro-burn using the Skylon Orbital Manoeuvring Assembly (SOMA) to reduce its velocity and commence descent. During descent, the vehicle adjusts both its angle of attack and roll angle to maintain the pre-calculated attitude conditions necessary to reach the predetermined spaceport while managing temperatures and heat flows. In the landing phase, Skylon will execute a gliding flight and, as a Horizontal Take-Off Landing (HTOL) vehicle, will perform a landing similar to that of the Space Shuttle. The high temperatures generated during the re-entry phase due to shock waves not only hold significant interest for the thermal and structural analysis of the vehicle but also profoundly impact the emission analysis. As mentioned in 4.1.2, the formation of nitrogen oxides (NO_x), by thermal way, does not require combustion; it is sufficient for the temperature to exceed 1800K. This threshold temperature, identified by Zeldovich [37], provides the minimum energy necessary to break the triple bonds holding nitrogen molecules (N_2) together.

The now free nitrogen atoms can bond with atomic and molecular oxygen, forming nitrogen oxides. In an effort to estimate the emissions produced during the re-entry phase, this chapter aims to replicate the analyses conducted by Park on the Space Shuttle re-entry [22, 23], updated for the new case study.

6.1 Analytical methods for estimating NO_x emissions

In the studies conducted on the Space Shuttle, first-approximation analytical methods were used, which allow for some initial results to be obtained with the knowledge of a few simple data points. In particular, knowing the mass and angle of incidence during the re-entry phase, it is possible to derive the nitrogen oxide emissions generated during the descent. The analytical methods considered in Park's original paper are the *trailing edge-freezing* and the *wake-freezing* models. The first one assumes that chemical reactions cease downstream of the vehicle's trailing edge due to the significant expansion that occurs. This approach is thought to be overly simplistic as it does not account for the high temperatures present in the wake, which can still promote chemical reactions. Therefore, the *wake-freezing* model is preferred in this analysis, as it considers that that reactions can occur even downstream of the vehicle's trailing edge. Additionally, it considers that the airflow impacted by the vehicle will mix with the surrounding atmosphere with which it can interact. Indeed, although there is a significant expansion downstream of the vehicle where the temperature decreases, turbulent mixing generates dissipation and further heating of the flow. In this method, at a certain distance from the vehicle's trailing edge, there will be a point where the temperature is low enough to prevent further reactions: this point is called the *freezing-point*. The following presents the chosen method for analysis to make it as understandable as possible. It is a two-step process: the first step involves calculating the mass fraction of NO generated at the *freezing-point* downstream of the vehicle. The second step involves calculating the mass of air impacted by the vehicle. This value is then multiplied by the *wake growth factor* (F), which accounts for the increase in cross-sectional area due to the interactions the wake has with the rest of the atmosphere. The validity of the method presented by Park depends on the vehicle being considered as a flat plate with a triangular shape, corresponding to the exposed surface area during the re-entry phase, which depends on the angle of attack maintained during the trajectory. Not knowing the trajectory of the Skylon and its angles of attack, it is assumed that they fall within a range equal to those of the Space Shuttle, which is between 25° and 40° depending on the phase of the trajectory.

The air impacted during re-entry can be estimated by considering the conservation of energy. Specifically, the contribution of drag on the vehicle is equated with

its change in kinetic energy:

$$\frac{1}{2} C_D \, \rho \, U^2 \, A \, ds \; = \; \frac{1}{2} M \, d(U^2)$$

Isolating the frontal area (A) and the density (ρ) and integrating the distance along the flight path, the following expression is obtained:

$$\int_{s_1}^{s_2} \rho \, A \, ds \; = \; 2 \, \frac{M}{C_D} \, \log \frac{U_1}{U_2} \tag{6.1}$$

where M denotes the mass of the vehicle during re-entry, which is assumed to be constant, while U_1 and U_2 represent the initial and final velocities, respectively. The final term to be calculated is the drag coefficient (C_D), which can be obtained using Newton's approximation applicable for hypersonic flows, specifically:

$$C_D \; = \; 2 \, \sin^2 \alpha$$

where α represents the angle of attack. In an effort to consider the worst-case scenario, the *freezing-point* was selected at the distance where the mass fraction of nitrogen oxides is maximized. Therefore, the mass fraction of NO_x is assumed to be constant during the descent phase and is equal to 1.951%. This value is obtained from the figure 6.1.

The product of the air swept by the vehicle, the wake growth factor, and the nitrogen oxide fraction yields the estimate of emissions generated during the re-entry phase. Specifically, the results obtained can be observed in Table 6.1.

6.2 Numerical analysis

After applying Park's method, a numerical analysis method will be employed to incorporate the available data and enable a more comprehensive analysis. To proceed in this direction, it is necessary to determine the trajectory of the Skylon. Although the exact trim is unknown, a first approximation trajectory can be derived from the data by sampling the descent trajectory shown in 3.3, based on time, altitude, and flight velocity. With these data, a more realistic analysis of Skylon's reentry phase can be generated. Using Park's approximations, the mass of air encountered by the vehicle can be calculated. The integral in the formula 6.1 is divided into all sampling intervals, and the mass of air encountered in each interval is determined. Having obtained the quantities of air swept by the aircraft, it is possible to proceed with the calculation of emissions. In particular, the Cantera software is again used, to which the atmosphere model, defined in 5.2, the kinetic model, the characteristics of the descent trajectory and the properties of the air downstream of the collisions are provided as input. Specifically, the kinetic model

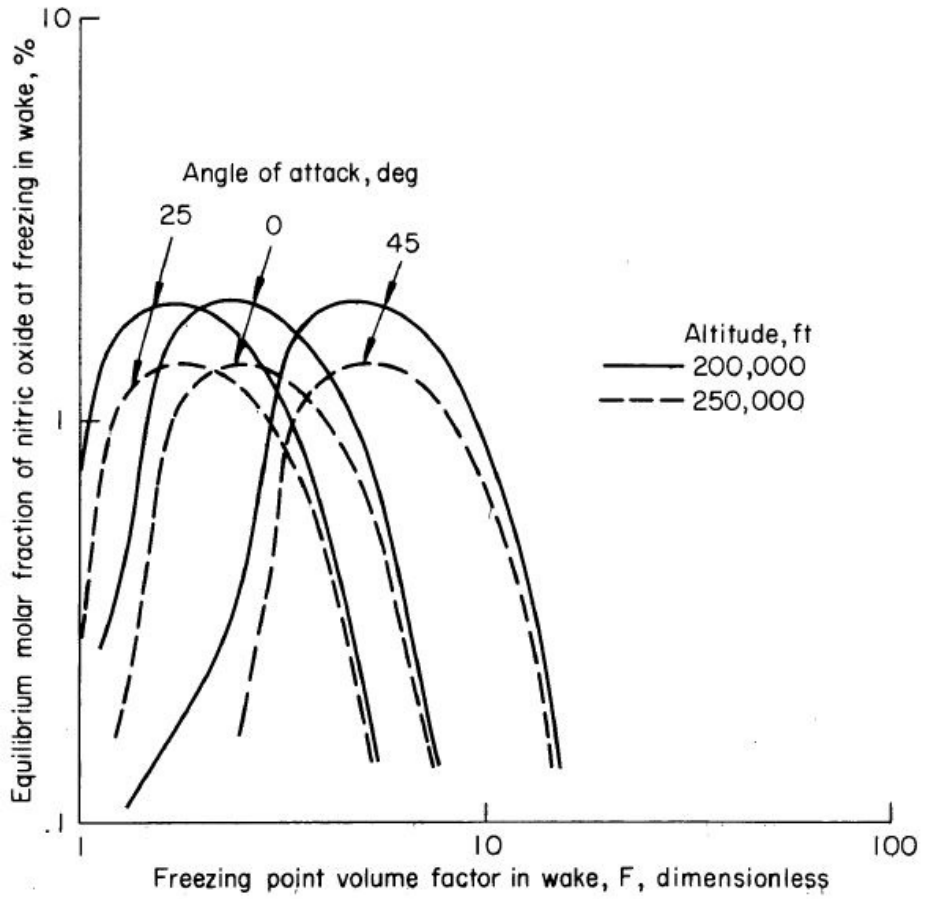

Figure 7.- Equilibrium molar fraction of NO at freezing point volume factor F. The volume factor F is the ratio of air mass in wake to the air mass swept by reentry vehicle (wake-freezing approximation).

Figure 6.1: Equilibrium molar fraction of NO at freezing point volume factor (F), [22]

used is the *airNASA9ions*, which is more suitable for this study than the *z24_NOx* previously used because, although it does not implement hydrogen, it considers molecules that are present in greater percentage in air, such as carbon oxides and argon, and also includes the ions of all the elements contained in the model. This turns out to be an important detail since, during the re-entry phase, the formation of plasma in the wake of the aircraft is typical. The study of the properties downstream of the shocks was carried out with the aid of Matlab's *Oblique Shock Calculator* library [26]. This function made it possible to calculate, given the angles

of incidence and the mach of flight, the deflection angle of the shock. It was then possible to decompose the flight mach into tangent and normal and resolve the normal shock. For an easier understanding of the procedure, the code has been reproduced in the appendix B.

The study of NO_x production in Cantera proceeds with the definition of two different air currents: the first is the Skylon impacted current. The quantity is equal to that calculated using the integral of Park divided by intervals and its thermodynamic properties are derived from the shock solutions. Instead, the second flow simulates the part of the atmosphere with which the hot flow interacts. Using the *EQUILIBRATE('HP')* command, the mixing of the two flows at constant pressure and enthalpy is obtained, and the solution under equilibrium conditions is derived. From the results, it was possible to derive the mass fractions of the nitrogen oxides for each sampling interval, and by simple multiplication with the total mass of air involved, it was possible to derive the atmospheric emissions, broken down by flight altitude, as can be seen in the figure 6.2.

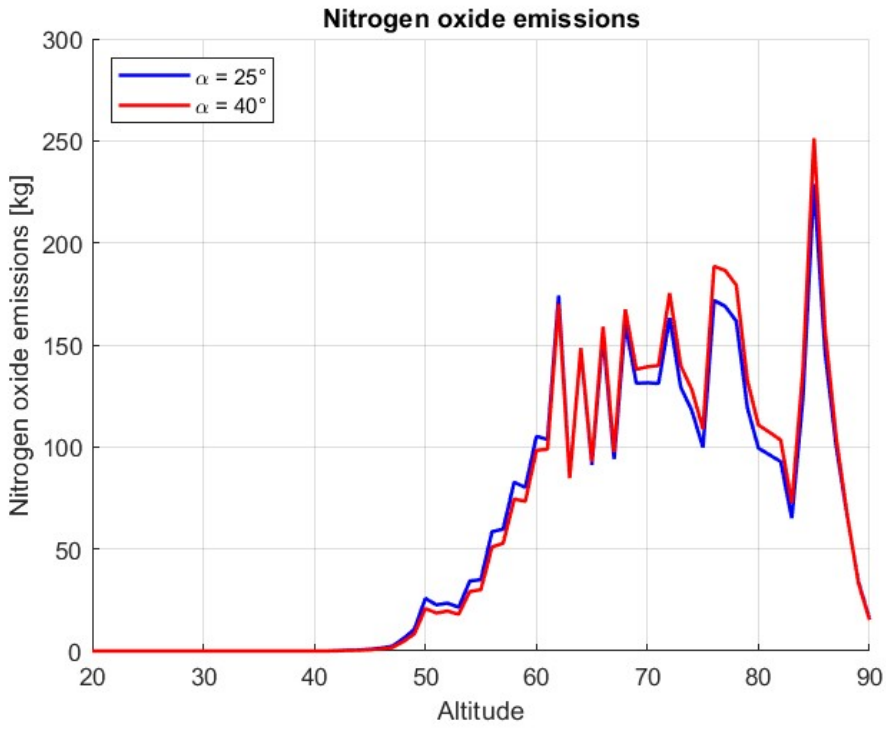

Figure 6.2: Nitrogen oxides produced during Skylon re-entry at different angles of attack as a function of altitude

In the table 6.1 it is possible to see the difference in emissions obtained through Park's method applied to the Skylon and the analytical method using Cantera.

Angle of attack	***Wake-freezing* method**	**Numerical analysis**
$\boldsymbol{\alpha = 25°}$	4215 [kg]	4176 [kg]
$\boldsymbol{\alpha = 40°}$	5056 [kg]	4336 [kg]

Table 6.1: Re-entry phase NO_x emissions obtained by the two proposed methods

Chapter 7

Conclusions

In an effort to reduce the environmental impact that the aerospace sector is increasingly pursuing, especially due to the growing demand for access to space, the present research undertook to develop a methodology capable of providing an estimate of the emissions generated during both the ascent and re-entry phases of a space access aircraft. Specifically, this work worked on three main aspects: the generation of a propulsion model and the corresponding database containing the performance of the engine under analysis, the generation of an emission database of the same engine and, finally, the analysis and environmental impact in the re-entry phase of the vehicle. The methodology developed was applied to the Synergetic Air-Breathing Rocket Engine (SABRE), an innovative engine being designed at Reaction Engines Limited (REL). This is a very promising combined-cycle technology: it is capable of operating in both air-breathing and rocket mode. It is on the latter part that the propulsion model was developed: specifically, as nothing exists in the literature, this model was built from the air-breathing configuration and then specialised on the rocket concept. In the formulation of the model, the typical assumptions of the ideal endoreactor model were made, especially in the modelling of the nozzle and the calculation of engine performance. From the results obtained from the modelling, it can be stated that the calculated performance is similar to that provided by the REL: in fact, no other databases are available which analyse this phase of the Skylon's flight in more detail with which to make a more detailed comparison. The realisation of the model was carried out in parallel on Matlab and Python in such a way as to exploit the maximum potential of both: specifically, the modelling in Matlab concerns the phases of the cycle prior to combustion. Instead, in Python, combustion was simulated using the specialised software Cantera, which carries out time-dependent simulations of chemical kinetics. Following the mixing and combustion simulation, a calculation of the performance and emissions generated as a result of combustion and mixing with the external environment was carried out in the same code. These turn out to be the input

data for the second main aspect analysed in this thesis work. In fact, the emission database was created by considering the composition of the exhaust gases and the behaviour they have in contact with the surrounding atmosphere. As a result of the analysis performed, there are several noteworthy findings. Specifically, it was found that methods for minimising nitrogen oxide emissions used in air-breathing engines are counterproductive when applied in rocket propulsion. Indeed, decreasing the residence time or lowering the Adiabatic Flame Temperature (AFT) in this case generates an increase in emissions. A further aspect is linked to the mixture ratio, in fact better performance and a decrease in emissions are noted in the case of a Mixture Ratio (MR) close to the stoichiometric one: the reason is linked to the fact that in this situation, the unburnt coming from the engine are almost null and consequently the reactions in the atmosphere are limited, vice versa, in the presence of unburnt hydrogen, the oxygen present in the atmosphere can react and generate an afterburner. In this case, nitrogen oxide emissions are orders of magnitude higher than in the stoichiometric case. The formation of water vapour is also much higher, which, as is known, is a climate-altering element, especially at high altitudes. It is particularly difficult to compare the emissions of nitrogen oxides with other simulations as there is still no analysis in the literature that can be compared to this in terms of the methodology proposed. Finally, the last aspect analysed in this thesis concerns the re-entry phase. Although it is often a neglected aspect during analyses, re-entry generates quantities of emissions that cannot be overlooked. The emissions generated during this phase are a consequence of re-entry into the atmosphere, and in particular of the interaction between the aircraft and the air, from which shock waves arise that heat the air strongly. This reaches very high temperatures, which favours the formation of nitrogen oxides. As reported in the analysis, the formation of nitrogen oxides during the descent phase is higher than those generated in the ascent phase, in a ratio of up to 40:1. To conclude, although this work is only a first approach to the realisation of a methodology for estimating emissions generated during the rocket phase of launchers and space access aircraft, it has proven to be accurate and replicable for other engine types. However, there is still room for improvement. In fact, the implementation of software capable of providing a trajectory, both ascending and descending, would allow significant benefits in estimating total emissions. Furthermore, by considering kinetic schemes that take into account a wider range of elements, it would be possible to obtain the emissions of other chemical species that have not been considered so far, such as carbon oxides in the re-entry phase. Finally, the realisation of a database, similar to the one realised by the International Civil Aviation Organization (ICAO) for civil aviation, would allow the application of the most popular models for emission estimation, such as $P_3 - T_3$ and Boeing Fuel Flow Method 2 (BFFM2), also to the field of space launchers, providing new and very flexible estimation methods.

Appendix A

Matlab codes for modeling the SABRE in rocket mode

Listing A.1: Hydrogen Circuit

```
function [] = Stazione_0_1(beta_H2_01)

%% Calcolo stazione 0-1
Ptot_H2_1=Ptot_H2_0*beta_H2_01;

% Proprietà idrogeno
H2_th.Tpcalc(Ttot_H2_0,Ptot_H2_0,0.0280445);
cv_H2_0=H2_th.cv;                                   % [J/kmol/k],
thermo li restituisce in questa unità di misura
cp_H2_0=H2_th.cp;                                   % [J/kmol/k]
v_H2_0=H2_th.v;
gamma_H2_0=cp_H2_0/cv_H2_0;
rho_H2_0=H2_th.Mw/v_H2_0;

%
-------------------------------------------------------------------------

% Prima iterazione
%
-------------------------------------------------------------------------


% Potenza necessaria alla turbopompa
P_LHP=mdot_H2.*(Ptot_H2_1-Ptot_H2_0)/(neta_compressore*rho_H2_0);
            % [W]

% Calcolo Temperatura con iterazione del calcolo per aggiornare
il gamma
```

```
22      Ttot_H2_1=Ttot_H2_0*+((1-neta_compressore)/neta_compressore).*(
    P_LHP./(mdot_H2*cp_H2_0/H2_th.Mw));
23
24      %
    ------------------------------------------------------------------------

25      % Calcolo iterativo
26      %
    ------------------------------------------------------------------------

27      for i=1:number_of_elements
28          error1=1;
29          error2=1;
30          while error1>toll || error2>toll
31              H2_th.Tpcalc(Ttot_H2_1(i),Ptot_H2_1(i))
32              cv_H2_1(i)=H2_th.cv;
33              cp_H2_1(i)=H2_th.cp;
34              cp_H2_01(i)=(cp_H2_1(i)+cp_H2_0)/2;
35              cv_H2_01(i)=(cv_H2_1(i)+cv_H2_0)/2;
36              v_H2_1(i)=H2_th.v;
37              rho_H2_01(i)=0.5*(H2_th.Mw/v_H2_0+H2_th.Mw/v_H2_1(i));
38              gamma_H2_01=cp_H2_01(i)/cv_H2_01(i);
39              P_LHP_new=mdot_H2(i)*(Ptot_H2_1-Ptot_H2_0)/(
    neta_compressore*rho_H2_01);
40              Ttot_H2_1_new=Ttot_H2_0+((1-neta_compressore)/
    neta_compressore)*(P_LHP_new/(mdot_H2(i)*cp_H2_01(i)/H2_th.Mw));
41              error2=abs(Ttot_H2_1_new-Ttot_H2_1(i))/Ttot_H2_1(i);
42              error1=abs(P_LHP_new-P_LHP(i))/P_LHP(i);
43              P_LHP(i)=P_LHP_new;
44              Ttot_H2_1(i)=Ttot_H2_1_new;
45          end
46      end
47
48  end
49
50
51  function [] = Stazione_1_2()
52
53      %% Calcolo stazione 1-2
54
55      %
    ------------------------------------------------------------------------

56      % Prima Iterazione
57      %
    ------------------------------------------------------------------------

58      Ptot_H2_2=Ptot_H2_1*eps_HX;
59      Ttot_H2_2=Ttot_H2_1+P_HX4./(mdot_H2.*cp_H2_1/H2_th.Mw);
```

```
60
61      %
        ------------------------------------------------------------------------

62      % Ciclo iterativo
63      %
        ------------------------------------------------------------------------

64      for i=1:number_of_elements
65          error=1;
66          while error>toll
67              H2_th.Tpcalc(Ttot_H2_2(i),Ptot_H2_2(i))
68              cv_H2_2(i)=H2_th.cv;
69              cp_H2_2(i)=H2_th.cp;
70              cp_H2_12(i)=(cp_H2_1(i)+cp_H2_2(i))/2;
71              cv_H2_12(i)=(cv_H2_1(i)+cv_H2_2(i))/2;
72              gamma_H2_12(i)=cp_H2_12(i)/cv_H2_12(i);
73              Ttot_H2_2_new=Ttot_H2_1(i)+P_HX4(i)/(mdot_H2(i)*cp_H2_12(
    i)/H2_th.Mw);
74              error=abs(Ttot_H2_2_new-Ttot_H2_2(i))/Ttot_H2_2(i);
75              Ttot_H2_2(i)=Ttot_H2_2_new;
76          end
77      end
78
79  end
80
81  function [] = Stazione_2_3(P_LHP)
82
83      %% Calcolo stazione 2-3
84
85      %
        ------------------------------------------------------------------------

86      % Prima iterazione
87      %
        ------------------------------------------------------------------------

88
89      % Calcolo della stazione 3: temperatura grazie all'uguaglianza
    delle
90      % potenze connesse all'albero e pressione
91      W_t_23=P_t_23./mdot_H2;        % Si ottiene il lavoro estratto in
    turbina
92      Ttot_H2_3=Ttot_H2_2-W_t_23./(cp_H2_2/H2_th.Mw);
93
94      %
        ------------------------------------------------------------------------

95      % Ciclo iterativo
```

```
96      %
        ------------------------------------------------------------------------

97
98      for i=1:number_of_elements
99          error=1;
100         while error>toll
101             H2_th.Tpcalc(Ttot_H2_3(i),Ptot_H2_3(i))
102             cv_H2_3(i)=H2_th.cv;
103             cp_H2_3(i)=H2_th.cp;
104             cp_H2_23(i)=(cp_H2_2(i)+cp_H2_3(i))/2;
105             cv_H2_23(i)=(cv_H2_2(i)+cv_H2_3(i))/2;
106             gamma_H2_23(i)=cp_H2_23/cv_H2_23;
107             Ttot_H2_3_new=Ttot_H2_2(i)-W_t_23(i)/(cp_H2_23(i)/H2_th.
    Mw);
108             error=abs(Ttot_H2_3_new-Ttot_H2_3(i))/Ttot_H2_3(i);
109             Ttot_H2_3(i)=Ttot_H2_3_new;
110             beta_t_23(i)=(1/neta_turbina*(Ttot_H2_3(i)/Ttot_H2_2(i)
    -1)+1)^(-gamma_H2_23(i)/(gamma_H2_23(i)-1));
111             Ptot_H2_3(i)=Ptot_H2_2(i)/beta_t_23(i);
112         end
113     end
114
115 end
116
117 function [] = Stazione_3_4(P_c_1112)
118
119     %% Calcolo stazione 3-4
120
121     %
        ------------------------------------------------------------------------

122     % Prima iterazione
123     %
        ------------------------------------------------------------------------

124
125     P_t_34=P_c_1112;
126     Ttot_H2_4=Ttot_H2_3-P_t_34./(mdot_H2.*cp_H2_3/H2_th.Mw);
127
128     %
        ------------------------------------------------------------------------

129     % Ciclo iterativo
130     %
        ------------------------------------------------------------------------

131
132     for i=1:number_of_elements
```

```
133             error=1;
134             while error>toll
135                 H2_th.Tpcalc(Ttot_H2_4(i),Ptot_H2_4)
136                 cv_H2_4(i)=H2_th.cv;
137                 cp_H2_4(i)=H2_th.cp;
138                 cp_H2_34(i)=(cp_H2_3(i)+cp_H2_4(i))/2;
139                 cv_H2_34(i)=(cv_H2_3(i)+cv_H2_4(i))/2;
140                 gamma_H2_34(i)=cp_H2_34/cv_H2_34;
141                 Ttot_H2_4_new=Ttot_H2_3(i)-P_t_34/(mdot_H2(i)*cp_H2_34(i)
    /H2_th.Mw);
142                 error=abs(Ttot_H2_4_new-Ttot_H2_4(i))/Ttot_H2_4(i);
143                 Ttot_H2_4(i)=Ttot_H2_4_new;
144                 beta_t_34(i)=((Ttot_H2_4(i)/Ttot_H2_3(i)-1)/neta_turbina
    +1)^(-gamma_H2_34/(gamma_H2_34-1));
145             end
146         end
147
148 end
```

Listing A.2: Oxygen Circuit

```
function [] = Stazione_5_6()
% Richiamo dei dati nei file appositi
DATI;
DATI_ELIO;
VARIABILI_GLOBALI;

% Valori stazione 5 calcolati tramite la classe Thermo.m
O2_th.Tpcalc(Ttot_O2_5,Ptot_O2_5,0.0280445);
cv_O2_5=O2_th.cv;                                   % [J/kmol/k], thermo li restituisce in questa unità di misura
cp_O2_5=O2_th.cp;                                   % [J/kmol/k]
v_O2_5=O2_th.v;
gamma_O2_5=cp_O2_5/cv_O2_5;
rho_O2_5=O2_th.Mw/v_O2_5;

beta_O2_56=(Pc/eps_HX)/(Ptot_O2_5);
Ptot_O2_6=beta_O2_56*Ptot_O2_5;
P_LOP=mdot_O2*(Ptot_O2_6-Ptot_O2_5)/(neta_compressore*rho_O2_5);


Ttot_O2_6=Ttot_O2_5+((1-neta_compressore)/neta_compressore)*(P_LOP./(mdot_O2*cp_O2_5/O2_th.Mw));

% Calcolo iterativo
for i=1:number_of_elements
    error=1;
    while error>toll
        O2_th.Tpcalc(Ttot_O2_6(i),Ptot_O2_6,0.0280445)
        cv_O2_6(i)=O2_th.cv;
        cp_O2_6(i)=O2_th.cp;
        cp_O2_56(i)=(cp_O2_6(i)+cp_O2_5)/2;
        cv_O2_56(i)=(cv_O2_6(i)+cv_O2_5)/2;
        v_O2_6(i)=O2_th.v;
        rho_O2_56(i)=0.5*(O2_th.Mw/v_O2_5+O2_th.Mw/v_O2_6(i));
        gamma_O2_56(i)=cp_O2_56(i)/cv_O2_56(i);
        Ttot_new=Ttot_O2_5+((1-neta_compressore)/neta_compressore)*(P_LOP(i)/(mdot_O2(i)*cp_O2_56(i)/O2_th.Mw));
        error=abs(Ttot_new-Ttot_O2_6(i))/Ttot_O2_6(i);
        Ttot_O2_6(i)=Ttot_new;
    end
end

end
```

Listing A.3: Helium Cycle

```
function [] = Ciclo_Elio(P_LOP)

% Richiamo dati generici
DATI;
DATI_ELIO;
VARIABILI_GLOBALI;

%% Calcolo ciclo dell'elio

Ptot_He_14=Ptot_He_11/eps_HX;   % Pressione ricavata considerando le perdite dovute allo scambiatore di calore
P_t_1314=P_LOP;                 % Impongo uguaglianza di potenza essendo collegati da un albero
W_t_1314=P_t_1314/mdot_He;      % Si ottiene il lavoro svolto (senza considerare la portata)

% Si effettua una prima iterazione con valori di riferimento alle
% temperature note dell'elio. In seguito questi valori verranno
% aggiornati considerando temperature e pressioni delle singole
% stazioni
Ttot_He_14=Ttot_He_13-W_t_1314/cp_He_12;
beta_t_1314=(1/neta_turbina*(Ttot_He_14./Ttot_He_13-1)+1).^(-gamma_He_12/(gamma_He_12-1));
Ptot_He_13=Ptot_He_14.*beta_t_1314;

Ptot_He_12=Ptot_He_13/eps_HX;

% Calcoliamo il rapporto di compressione che c'è nel compressore del
% circuito dell'elio tra le stazioni 12 e 13
beta_c_1112=Ptot_He_12./Ptot_He_11;

% Calcolo della Ttot_He_12 mediante il rapporto di compressione e calcolo
% della potenza necessaria per compiere la compressione dell'elio (sarà la
% medesima potenza da estrarre dall'idrogeno per poter lavorare)

Ttot_He_12=Ttot_He_11.*(1+1/neta_compressore.*(beta_c_1112.^((gamma_He_12-1)/gamma_He_12)-1));

P_c_1112=mdot_He*cp_He_11*(Ttot_He_12-Ttot_He_11);

% Calcolo della potenza estratta nell'HX Nozzle

P_HX_Nozzle=mdot_He*cp_He_12*(Ttot_He_13-Ttot_He_12);

```

```
40  %
    ------------------------------------------------------------------------

41  % FINE PRIMA ITERAZIONE
42  %
    ------------------------------------------------------------------------

43
44  %% VARIABILI AUSILIARIE
45
46  cv_He_13=zeros(1,number_of_elements);
47  cp_He_13=zeros(1,number_of_elements);
48  gamma_He_13=zeros(1,number_of_elements);
49  cv_He_14=zeros(1,number_of_elements);
50  cp_He_14=zeros(1,number_of_elements);
51  gamma_He_14=zeros(1,number_of_elements);
52  Ttot_He_12_new=zeros(1,number_of_elements);
53
54  %% CICLO ITERATIVO
55
56  % Ciclo per iterare più volte tutto il conto
57  out=0;
58  while out==0
59
60      % Espansione in turbina - Stazione 13-14
61      for i=1:number_of_elements
62          error1=1;
63          error2=1;
64          while error1>toll || error2>toll
65
66              % Calcolo con cantera del cp e del cv nella stazione
    13
67              set(He,'T', Ttot_He_13(i), 'P', Ptot_He_13(i));
68              equilibrate(He,'TP');
69              cv_13=cv_mass(He);
70              cp_13=cp_mass(He);
71              gamma_13=cp_13/cv_13;
72
73              % Calcolo con CANTERA del cp e del cv nella stazione
    14
74              set(He,'T', Ttot_He_14(i), 'P', Ptot_He_14(i));
75              equilibrate(He,'TP');
76              cv_14=cv_mass(He);
77              cp_14=cp_mass(He);
78              gamma_14=cp_14/cv_14;
79
80              cp_medio=(cp_13+cp_14)/2;
81              cv_medio=(cv_13+cv_14)/2;
82              gamma_medio=(gamma_13+gamma_14)/2;
```

```
83
84                  % Calcolo Temp Tot stazione 14
85                  Ttot_He_14_new=Ttot_He_13(i)-W_t_1314(i)/cp_medio;
86                  error1=abs(Ttot_He_14_new-Ttot_He_14(i))/Ttot_He_14(i
    );
87                  Ttot_He_14(i)=Ttot_He_14_new;
88
89                  % Calcolo Espansione della turbina 13-14
90                  beta_t=(1/neta_turbina*(Ttot_He_14(i)/Ttot_He_13(i)
    -1)+1).^(-gamma_medio/(gamma_medio-1));
91                  error2=abs(beta_t_1314(i)-beta_t)/beta_t_1314(i);
92                  beta_t_1314(i)=beta_t;
93
94                  % Calcolo della pressione nella stazione 13 e 12
95                  Ptot_He_13(i)=Ptot_He_14(i)*beta_t_1314(i);
96                  Ptot_He_12(i)=Ptot_He_13(i)/eps_HX;
97
98                  % Calcoliamo il rapporto di compressione che c'è nel
    compressore del
99                  % circuito dell'elio tra le stazioni 12 e 13
100                 beta_c_1112(i)=Ptot_He_12(i)/Ptot_He_11(i);
101
102                 % Calcolo della Ttot_He_12 mediante il rapporto di
    compressione e calcolo
103                 % della potenza necessaria per compiere la
    compressione dell'elio (sarà la
104                 % medesima potenza da estrarre dall'idrogeno per
    poter lavorare)
105                 Ttot_He_12_new(i)=Ttot_He_11(i)*(1+1/neta_compressore
    *(beta_c_1112(i).^((gamma_medio_1112-1)/gamma_medio_1112)-1));
106                 P_c_1112=mdot_He*cp_medio_1112*(Ttot_He_12_new(i)-
    Ttot_He_11(i));
107
108             end
109
110             % Si segnano i valori aggiornati dei calori specifici
111             cv_He_13(i)=cv_13;
112             cp_He_13(i)=cp_13;
113
114             cv_He_14(i)=cv_14;
115             cp_He_14(i)=cp_14;
116         end
117
118         if abs(Ttot_He_12_new-Ttot_He_12)/Ttot_He_12<toll
119             out=1;
120         else
121             Ttot_He_12=Ttot_He_12_new;
122             Ttot_He_12_new=0;
123         end
```

```
124     end
125
126     % Calcolo della potenza estratta nello scambiatore di calore HX4
127     cp_He_1411=(cp_He_14+cp_He_11)/2;
128     P_HX4=mdot_He*cp_He_1411.*(Ttot_He_14-Ttot_He_11);
129
130     % Calcolo della potenza, nonchè calore, estratto nell'ugello
131     P_HX_Nozzle=mdot_He.*((cp_He_13+cp_He_12)/2).*(Ttot_He_13-
        Ttot_He_12);
132
133 end
```

Appendix B

Matlab code for modeling the reentry phase of the Skylon

Listing B.1: Shock Wave resolution

```
1
2       %% Definiamo i dati
3   gamma = 1.4;                        % Si assume costante perchè aria in
        quiete
4   theta = [25, 40];                   % gradi di angolo di attacco
5   Cd=2*(sind(theta)).^2;
6
7   Superficie_skylon = 690.13;         % [m2]
8   Sup_frontale_25=Superficie_skylon*sind(theta(1));
9   Sup_frontale_40=Superficie_skylon*sind(theta(2));
10  mass_skylon=53.4*1e3*1.01;  % [kg]
11
12  beta25= zeros(length(Traiettoria_rientro.Mach),1);
13  beta40= zeros(length(Traiettoria_rientro.Mach),1);
14
15  M1n_25= zeros(length(Traiettoria_rientro.Mach),1);
16  M1n_40= zeros(length(Traiettoria_rientro.Mach),1);
17
18  P_25= zeros(length(Traiettoria_rientro.Mach),1);
19  T_25= zeros(length(Traiettoria_rientro.Mach),1);
20
21  P_40= zeros(length(Traiettoria_rientro.Mach),1);
22  T_40= zeros(length(Traiettoria_rientro.Mach),1);
23
24  %% Calcolo beta e mach normale della lamina
```

```
25
26 M1=Traiettoria_rientro.Mach;
27
28 % Calcolo dei mach normali all'urto obliquo
29 for i=1:length(Traiettoria_rientro.Mach)
30
31     % 25 gradi
32     if i<1014
33         [beta25(i) ,~] = oblique_angle_calc (M1(i) ,'mach', theta(1)
    ,'theta',gamma);
34         M1n_25(i)=M1(i)*sind(beta25(i));
35         [~, T_25(i), P_25(i), ~, ~,~,~]= flownormalshock(gamma,
    M1n_25(i), 'mach');
36     else
37         [~, T_25(i), P_25(i), ~, ~,~,~]= flownormalshock(gamma, M1(i)
    , 'mach');
38     end
39
40     % 40 gradi
41     if i<962
42         [beta40(i) ,~] = oblique_angle_calc (M1(i) ,'mach', theta(2)
    ,'theta',gamma);
43         M1n_40(i)=M1(i)*sind(beta40(i));
44         [~, T_40(i), P_40(i), ~, ~,~,~]= flownormalshock(gamma,
    M1n_40(i), 'mach');
45     else
46         [~, T_40(i), P_40(i), ~, ~,~,~]= flownormalshock(gamma, M1(i)
    , 'mach');
47     end
48
49 end
50
51 %% Calcolo massa d'aria investita in ogni sezione della traiettoria
52
53 %air_mass=2*(mass_skylon*log(U(1)/U(2)))./Cd; % [kg] come il peso
    dello skylon
54 massa_investita_25 = [2*(mass_skylon* abs(log(Traiettoria_rientro.
    Mach(1:end-1)./Traiettoria_rientro.Mach(2:end))))/Cd(1); 0];
55 massa_investita_40 = [2*(mass_skylon* abs(log(Traiettoria_rientro.
    Mach(1:end-1)./Traiettoria_rientro.Mach(2:end))))/Cd(2); 0];
56
57 massa_scia_25=massa_investita_25*F_25;
58 massa_scia_40=massa_investita_40*F_40;
```

Bibliography

[1] NASA. URL: https://cearun.grc.nasa.gov/index.html.

[2] URL: https://www.atag.org/facts-figures/.

[3] Alejandro Block and Thomas Rötger. «Liquid Hydrogen as a Potential Low-Carbon Fuel for Aviation». In: (Aug. 2019). URL: https://www.iata.org/contentassets/d13875e9ed784f75bac90f000760e998/fact_sheet7-hydrogen-fact-sheet_072020.pdf.

[4] https://www.icao.int/environmental-protection/CORSIA/Pages/default.aspx.

[5] N. Chandrasekaran and Abhijit Guha. «Study of Prediction Methods for NOx Emission from Turbofan Engines». In: *JOURNAL OF PROPULSION AND POWER* Vol. 28, No. 1 (Feb. 2012). DOI: 10.2514/1.B34245.

[6] J.W. Cornelisse, H.F.R. Schöyer, and K.F. Wakker. *Rocket Propulsion and Spaceflight Dynamics*. Aerospace Engineering Series pt. 1. Pitman, 1979. ISBN: 9780273011415. URL: https://books.google.it/books?id=HpJTAAAAMAAJ.

[7] J.A. Dallas, S. Raval, J.P. Alvarez Gaitan, S. Saydam, and A.G. Dempster. «The environmental impact of emissions from space launches: A comprehensive review». In: *Journal of Cleaner Production* 255 (2020), p. 120209. DOI: 10.1016/j.jclepro.2020.120209.

[8] Roberta Fusaro, Guido Saccone, and Nicole Viola. «NOx emissions estimation methodology for air-breathing reusable access to space vehicle in conceptual design». In: *Acta Astronautica* 216 (2024), pp. 304–317. DOI: https://doi.org/10.1016/j.actaastro.2023.12.060.

[9] Giovanni Grimaldi. *Development of a conceptual design tool to predict performance and pollutant and GHG emissions of high-speed vehicles using liquid hydrogen*. Dec. 2021.

[10] Mark Hempsell, Roger Longstaff, and Varvill. *Skylon User's Manual*. Reaction Engines Limited. 2014. URL: https://forum.nasaspaceflight.com/index.php?action=dlattach;topic=57281.0;attach=2130072.

[11] P.G. Hill and C.R. Peterson. *Mechanics and Thermodynamics of Propulsion*. Addison-Wesley Longman, 2010. ISBN: 9780132465489. URL: https://books.google.it/books?id=8ihcPgAACAAJ.

[12] Antonella Ingenito. «Impact of hydrogen fueled hypersonic airliners on the O3 layer depletion». In: *International Journal of Hydrogen Energy* 43.50 (2018), pp. 22694–22704. DOI: https://doi.org/10.1016/j.ijhydene.2018.09.208.

[13] Michael M. J., Alexandria R. S., Matthew F. C., and Shane V. L. *Launch Vehicle Noise and Emissions Simulation Model: User guide*. 2020. URL: https://onlinepubs.trb.org/onlinepubs/acrp/acrp_wod_051RumbleGuide.pdf.

[14] Michael M. James, Shane V. Lympany, Alexandria R. Salton, Matthew F. Calton, Blue Ridge Research, Consulting, LLC, Richard C. Miake-Lye, Inc. Aerodyne Research, and AECOM Roger L. Wayson. *Commercial Space Vehicle Emissions Modeling (2021)*. Tech. rep. National Academies of Science, Engineering and Medicine, 2022. DOI: 10.17226/26142.

[15] Khushin Lakhara, Rupesh Aggarwal, Tocky Darang, Naman Jain, Siddharth Gangly, and P. Sharma. «SABRE ENGINE: Single Stage to Orbit Rocket Engine». In: *International Journal of Innovative Research in Science, Engineering and Technology* 4 (Nov. 2015), p. 10360.

[16] Erik J. L. Larson, RobertW. Portmann, Karen H. Rosenlof, DavidW. Fahey, John S. Daniel, and Martin N. Ross. «Global atmospheric response to emissions froma proposed reusable space launch system». In: *AGU Earth's Future* (2017). DOI: 10.1002/2016EF000399.

[17] Sigrun Matthes, David Lee, Ruben Rodriguez De Leon, Ling Lim, Bethan Owen, Agnieszka Skowron, Robin Thor, and Etienne Terrenoire. «Review: The Effects of Supersonic Aviation on Ozone and Climate». In: *Aerospace* 9 (Jan. 2022), p. 41. DOI: 10.3390/aerospace9010041.

[18] Unmeel Mehta, Michael Aftosmis, Jeffrey Bowles, and Shishir Pandya. «Skylon Aerodynamics and SABRE Plumes». In: (July 2015). DOI: 10.2514/6.2015-3605.

[19] A. Mjaavatten. *User guide for matlab class thermo*. 2020. URL: https://github.com/are-mj/thermodynamics.

[20] Simone Moino. *Methodology and tools for propulsive performance characterization of high-speed aircraft in conceptual design*. 2021.

[21] *National Institute of Standard and Technology (NIST) Database*. URL: https://webbook.nist.gov/chemistry/fluid/.

[22] Chul Park. «Estimates of nitric oxide production for lifting spacecraft reentry». In: *Atmospheric Environment* Vol. 10, pp. 309-313 (Sept. 1975). DOI: 10.1016/0004-6981(76)90171-2.

[23] Chul Park. «Equivalent-Cone calculation og nitric oxide production rate during space shuttle re-entry». In: *Atmospheric Environment* Vol. 14, pp. 971-972 (Oct. 1979). DOI: 10.1016/0004-6981(80)90011-6.

[24] Martin Ross, Darin Toohey, Manfred Peinemann, and Patrick Ross. «Limits on the Space Launch Market Related to Stratospheric Ozone Depletion». In: *Astropolitics* Vol. 7:1, pp. 52-82 (Mar. 2009). DOI: 10.1080/14777620902768867.

[25] Martin N. Ross and Patti M. Sheaffer. «Radiative forcing caused by rocket engine emissions». In: *AGU Earth's Future* Vol. 2, pp. 177-196 (Apr. 2014). DOI: 10.1002/2013EF000160.

[26] J. Ryan. *Oblique Shock Calculator*. 2013. URL: https://www.mathworks.com/matlabcentral/fileexchange/44756-oblique-shock-calculator.

[27] G. Saccone. *Hydrogen/air combustion phenomena characterization and emissions estimation*. Italian Aerospace Research Centre. June 2022.

[28] Elwyn Sirieys, Chloe Gentgen, Asha Jain, Julia Milton, and Olivier L. de Weck. «Space sustainability isn't just about space debris: On the atmospheric impact of space launches». In: *MIT Science Policy Review* (Aug. 2022). DOI: 10.38105/spr.whfig18hta.

[29] Morgan Stanley. *Space: Investing in the final frontier*. Oct. 2023. URL: https://www.morganstanley.com/ideas/investing-in-space.

[30] G.P. Sutton and O. Biblarz. *Rocket Propulsion Elements*. A Wiley Interscience publication. Wiley, 2001. ISBN: 9780471326427. URL: https://books.google.it/books?id=LQbDOxg3XZcC.

[31] Kieran N. Tait, Mohammad Anwar H. Khan, Steve Bullock, Mark H. Lowenberg, and Dudley E. Shallcross. «Aircraft Emissions, Their Plume-Scale Effects, and the Spatio-Temporal Sensitivity of the Atmospheric Response: A Review». In: *Aerospace* (July 2022). DOI: 10.3390/aerospace9070355.

[32] Victor Fernandez Villacé. *Simulation, Design and Analysis of Air-Breathing Combined-Cycle Engines for High-Speed Propulsion*. 2013.

[33] Ch. Voigt, U. Schumann, K. Graf, and K.-D. Gottschaldt. «IMPACT OF ROCKET EXHAUST PLUMES ON ATMOSPHERIC COMPOSITION AND CLIMATE ¡ AN OVERVIEW». In: *Progress in Propulsion Physics* Vol. 4, pp. 657-670 (2013). DOI: 10.1051/eucass/201304657.

[34] J. Warnatz, U. Maas, and R.W. Dibble. *Combustion: Physical and Chemical Fundamentals, Modeling and Simulation, Experiments, Pollutant Formation*. Springer Berlin Heidelberg, 2006. ISBN: 9783540453635. URL: https://books.google.it/books?id=CAMFwje5WOQC.

[35] Darryn Waugh and Timothy Hall. «AGE OF STRATOSPHERIC AIR: THEORY, OBSERVATIONS, AND MODELS». In: *Reviews of Geophysics* 40.4 (2002), pp. 1-1-1–26. DOI: https://doi.org/10.1029/2000RG000101. eprint: https://agupubs.onlinelibrary.wiley.com/doi/pdf/10.1029/2000RG000101. URL: https://agupubs.onlinelibrary.wiley.com/doi/abs/10.1029/2000RG000101.

[36] P. W. White and J. Hoffman. *Earth Global Reference Atmospheric Model (Earth-GRAM): User Guide*. 2021. URL: https://github.com/are-mj/thermodynamics.

[37] Y. B. Zeldovich, P. Y. Sadonikov, and A. Frank-Kamenerskij. *Oxidation of nitrogen in combustion*. 1947.

[38] Jianqiang Zhang, Zhenguo Wang, and Qinglian Li. «Thermodynamic efficiency analysis and cycle optimization of deeply precooled combined cycle engine in the air-breathing mode». In: *Acta Astronautica* (2017). DOI: 10.1016/j.actaastro.2017.06.011.